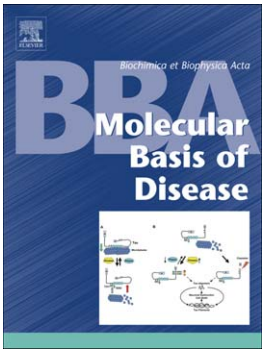

Imaging of Neuroinflammation in Alzheimer's Disease, Multiple Sclerosis and Stroke: Recent Developments in Positron Emission Tomography

Bieneke Janssen, Danielle J. Vugts, Uta Funke, Ger T. Molenaar, Perry S. Kruijer, Bart N.M. van Berckel, Adriaan A. Lammertsma, Albert D. Windhorst

PII: S0925-4439(15)00350-6
DOI: doi: 10.1016/j.bbadis.2015.11.011
Reference: BBADIS 64369

To appear in: *BBA - Molecular Basis of Disease*

Received date: 17 July 2015
Revised date: 9 October 2015
Accepted date: 19 November 2015

Please cite this article as: Bieneke Janssen, Danielle J. Vugts, Uta Funke, Ger T. Molenaar, Perry S. Kruijer, Bart N.M. van Berckel, Adriaan A. Lammertsma, Albert D. Windhorst, Imaging of Neuroinflammation in Alzheimer's Disease, Multiple Sclerosis and Stroke: Recent Developments in Positron Emission Tomography, *BBA - Molecular Basis of Disease* (2015), doi: 10.1016/j.bbadis.2015.11.011

Imaging of Neuroinflammation in Alzheimer's Disease, Multiple Sclerosis and Stroke: Recent Developments in Positron Emission Tomography

Bieneke Janssen[a], Danielle J. Vugts[a], Uta Funke[a,b], Ger T. Molenaar[a,b], Perry S. Kruijer[b], Bart N.M. van Berckel[a], Adriaan A. Lammertsma[a], Albert D. Windhorst[a]

[a] Department of Radiology & Nuclear Medicine, VU University Medical Center, Amsterdam, the Netherlands

[b] BV Cyclotron VU, Amsterdam, the Netherlands

Corresponding authors: Bieneke Janssen / Albert D. Windhorst

Radionuclide Center, Department of Radiology & Nuclear Medicine, VU University Medical Center, De Boelelaan 1085c, 1081 HV, Amsterdam, the Netherlands.

E-mail address: b.janssen@vumc.nl / ad.windhorst@vumc.nl

Telephone number: +31 (0)20-4449101

Fax: +31 (0)20-4449121

Abstract

Neuroinflammation is thought to play a pivotal role in many diseases affecting the brain, including Alzheimer's disease, multiple sclerosis and stroke. Neuroinflammation is characterised predominantly by microglial activation, which can be visualised using positron emission tomography (PET). Traditionally, translocator protein 18 kDa (TSPO) is the target for imaging of neuroinflammation using PET. In this review, recent preclinical and clinical research using PET in Alzheimer's disease, multiple sclerosis and stroke is summarised. In addition, new molecular targets for imaging of neuroinflammation, such as monoamine oxidases, adenosine receptors and cannabinoid receptor type 2, are discussed.

Highlights

- PET imaging of neuroinflammation is of high interest in AD, MS and stroke
- Recent preclinical and clinical PET research is summarised
- There is still room for improvement in tracer development for imaging of microglia

Keywords: positron emission tomography, neuroinflammation, microglia, Alzheimer's disease, multiple sclerosis, stroke

1. Introduction

Neuroinflammation is thought to play a pivotal role in many diseases affecting the brain, including Alzheimer's disease (AD), multiple sclerosis (MS) and stroke. Neuroinflammation is primarily characterised by microglial activation, although astrocytosis is also linked to neuroinflammation. Microglia are the primary immune effector cells of the brain, displaying a dual role in the immune response. Upon injury and/or release of inflammatory factors, microglia switch from a resting ramified state to an activated amoeboid state. This activation can be either pro- or anti-inflammatory, or, more likely, a combination of both states [1,2]. The general hypothesis is that initial microglial activation is beneficial for recovery of the injured central nervous system (CNS), e.g. by scavenging dead cells and secretion of neuron survival factors. On the other hand, prolonged microglial activation may lead, either directly or indirectly, to neuronal cell death [3]. Ideally, one would like to be able to distinguish between pro- and anti-inflammatory phenotypes of activated microglia *in vivo*, as this could affect disease treatment. The best technique to study microglial activation *in vivo* is positron emission tomography (PET). This imaging technique requires molecules labelled with a positron emitting isotope (tracers), targeting receptors, enzymes or other biomolecules showing increased expression in activated microglia. Traditionally, the translocator protein 18 kDa (TSPO) has been the target for imaging neuroinflammation using PET, with over 80 (and counting) tracers being developed with high affinity for TSPO. Some of these tracers have been evaluated in preclinical studies using different disease models of neuroinflammation, but (*R*)-[^{11}C]PK11195 still is the tracer most used in clinical research, despite of its low brain uptake and relatively high non-specific binding [4]. This is mainly due to the fact that (*R*)-[^{11}C]PK11195, unlike most second generation TSPO tracers, is not affected by binding differences due to two existing forms of TSPO, encoded by the rs6971 single-nucleotide polymorphism (SNP). In Caucasians, this polymorphism leads to prevalence of 49% high affinity binders (HABs), 42% mixed affinity binders (MABs) and 9% low affinity binders (LABs). Difference in binding was exemplified by Kreisl *et al*. using second generation TSPO tracer [^{11}C]PBR28 in healthy volunteers. Total distribution volume (V_T) of [^{11}C]PBR28 was reported to be 40% higher in brain of HABs than in brain of MABs. Additionally, autoradiography studies with [^{3}H]PBR28 on post-mortem samples of 45 schizophrenia patients and 47 control subjects (all genotyped) pointed out that tracer binding was increased with 16% in

schizophrenia patients. Importantly, this difference in tracer binding was only statistically significant when stratifying for genotype [5]. Therefore, the effect of the polymorphism needs to be kept in mind when quantifying TSPO PET images in human. Although not sensitive to polymorphism, (*R*)-[^{11}C]PK11195 suffers from low signal-to-noise ratios, therefore the search for better TSPO ligands still continues. As TSPO is not only overexpressed in activated microglia, but also in reactive astrocytes [6], there is a need for novel PET ligands that could distinguish between the two. In addition, visualisation of different microglial phenotypes may elucidate their role in disease onset and progression in neurodegenerative disease. PET ligands targeting other targets of neuroinflammation are being more and more explored, e.g. monoamine oxidase B (MAO-B), adenosine receptors, cannabinoid receptor type 2 (CB2) and matrix metalloproteinases (MMP) 2 and 9. PET imaging of neuroinflammation in AD, MS and stroke has been reviewed extensively in the past few years [3, 7-21]. The purpose of the present review is to summarise more recent advances (2013 – June 2015) in PET imaging of neuroinflammation in these diseases (table 1), starting with studies using tracers targeting TSPO. In addition, this review describes both existing and emerging targets with a focus on tracer development.

2. Tracers targeting translocator protein 18 kDa in healthy volunteers

In a blockade study in 26 healthy volunteers (all genotyped), [^{11}C]PBR28 PET scans were acquired [22]. Total volume of distribution (V_T) was found to be 1.5-fold higher in HABs compared with MABs in all regions of interest (ROIs) examined (cortex, hippocampus, thalamus, cerebellum, brain stem, striatum). Owen *et al.* then determined the non-displaceable volume of distribution (V_{ND}) of [^{11}C]PBR28 by blockade with XBD173 (TSPO ligand) in 6 HAB healthy volunteers. Each volunteer received a different dose of XBD173 (10-90 mg) orally, 2 hours prior to a repeat scan with [^{11}C]PBR28. Whole brain V_T in HABs was 4.33 ± 0.29 (n=16) and a measurable occupancy of TSPO in 5 out of 6 subjects was observed. The population V_{ND} was estimated to be 1.98 (1.69-2.26) via the occupancy plot. Authors conclude that a substantial part of [^{11}C]PBR28 specific binding in healthy subjects is represented by V_T; however, V_{ND} is almost half of V_T, complicating quantification of the specific binding. Based on a polymorphism plot using V_{ND} in HABs from the occupancy study, non-displaceable binding potential (BP_{ND}) was estimated to be 2-fold higher in HABs compared with MABs [22]. In another study, focused on modelling of [^{11}C]PBR28, the two-tissue compartment model (2TCM) with irreversible vascular trapping (2TCM-1K) was compared with 2TCM, which is usually used for TSPO ligands, using two previously acquired datasets [23]. 2TCM-1K V_T showed higher correlation with gene expression than 2TCM V_T and between-subject variability of absolute V_T values across brain regions was smaller using 2TCM-1K [23]. Simulated TACs based on the obtained

datasets showed 2TCM to severely underestimate increases in $V_{T,}$ leading to subtle changes not being observed (e.g. neuroinflammation). Binding of TSPO tracers in the vasculature has been shown previously [24]. However, 2TCM-1K suggests irreversible tracer binding to the vasculature, whereas binding to TSPO is known to be reversible. This indicates that the vascular target may not necessarily be TSPO, or that tracer kinetics in endothelium differ substantially from kinetics in brain parenchyma. In addition, inclusion of more parameters usually provides better fits, even if the additional parameters have limited physiological meaning. Therefore this extended model should first be validated using biological data, e.g. immunohistochemical staining and demonstration of irreversible binding in the vasculature.

Guo *et al*. showed slower [^{18}F]PBR111 washout from brain stem in HABs than in MABs and LABs (decrease of 50% at 60 (HAB), 40 (MAB) and 20 min (LAB) p.i.) in a group of 21 genotyped healthy volunteers (9 HABs, 8 MABs and 4 LABs) [25]. Thirty minutes after [^{18}F]PBR111 injection, 40% of the tracer was still intact, which decreased to 20% at 120 min p.i. The free fraction in plasma was not significantly different between genotype groups. Substantial variability in V_T was observed within each genotype group, especially in HABs (e.g. 2TC V_T (brain stem) HAB 5.08 ± 1.80; MAB 3.10 ± 0.50; LAB 2.33 ± 0.52), which the authors partly attribute to age [25]. Microglial activation, or at least TSPO overexpression, has also been shown to be increased upon healthy ageing using other TSPO-PET tracers [26,27,28]. In another cohort of 33 genotyped healthy volunteers (22 HABs, 11 MABs, 19-78 years old) using [^{18}F]FEPPA, no significant correlation between age and ROI (white matter; WM) or genotype and ROI (WM) was found among several grey and white matter brain regions [29,30]. Although not significantly different, V_T was 15% higher in HABs than in MABs. These studies in humans using different second generation TSPO tracers again demonstrate the importance of stratifying subjects for genotype, as differences (or no differences) between healthy subjects and patients may otherwise be due to different proportions of HABs and MABs.

[TABLE 1]

3. Alzheimer's Disease

Alzheimer's disease (AD) is a neurodegenerative disease characterized by cognitive as well as functional decline. The degree of cognitive decline, as well as its progression, is often monitored using the Mini Mental State Examination (MMSE). Neuropathological hallmarks of AD include extracellular deposition of amyloid β (Aβ), intracellular deposition of tau protein (neurofibrillary tangles) and neuroinflammation. Microglia can be activated by Aβ, and are thought to be involved in clearance of soluble Aβ oligomers by phagocytosis. Pro-inflammatory activation of microglia is accompanied by impaired function of phagocytosis, whereas in the anti-inflammatory phenotype, phagocytic function is increased [1]. Depending on disease stage, microglia may have different roles and due to the continued presence of Aβ it is likely that a chronic, non-resolving inflammation is present in AD [1]. Therefore, next to imaging of the deposition of Aβ and tau protein, imaging of neuroinflammation is thought to be important for monitoring disease onset and progression. The use of PET tracers in AD has been extensively reviewed over the years (most recent reviews: 7,8,16,17,19]), conveying that conflicting results have been obtained with respect to neuroinflammation imaging in AD, especially with respect to correlation with clinical disease score and protein deposition.

3.1 Preclinical PET research in animal models of Alzheimer's disease

The most widely used animal models of AD are transgenic (Tg) mice overproducing different strains of mutant familial amyloid precursor protein (APP). Disease onset and progression in APP Tg mice mimic the disease course and pathology in human AD and support the amyloid cascade hypothesis, although, in general, neuroinflammation is observed to a lesser extent in Tg models [31]. Below, studies using TSPO tracers in different APP Tg models will be discussed.

A PET study using *(R)*-[^{11}C]PK11195 (fig. 1) showed no statistical difference in tracer uptake between 13-month-old APP/PS1 Tg and wild type (wt) mice [32]. Immunohistochemical staining for CD11b (microglia marker) confirmed presence of activated microglia surrounding Aβ plaques in Tg mice, but not in wt mice, indicating that the amount of microglial activation in mice may be below the detection limit of *(R)*-[^{11}C]PK11195 microPET [32]. In addition, five weeks after discontinuation of five weeks of pioglitazone (PPAR-γ agonist) treatment, significantly higher *(R)*-[^{11}C]PK11195 distribution volumes were observed in 15-month-old Tg mice [32]. The authors concluded that this could indicate either natural disease progression or "rebound" microglial activation. However, non-treated 15-month-old Tg mice were not included in this study, so their conclusion remains debateable. Another study using [^{18}F]DPA-714 failed to show a significant difference in cerebral tracer uptake between APPswePS1dE9 Tg and wt mice at any age, even though mice were

longitudinally followed up until 19 months of age [33]. [^{18}F]DPA-714 standardized uptake value (SUV) ratios (SUVr; with cerebellum as reference region) were increased in cortex of 12- (1.05 ± 0.04 vs. 0.85 ± 0.05) and 19-month-old (1.02 ± 0.03 vs. 0.82 ± 0.04) Tg mice, but not in that of 15-month-old Tg mice (0.99 ± 0.03 vs. 0.82 vs. 0.05). In the hippocampus, critical for learning and memory and therefore an important ROI in AD, significantly increased tracer uptake was found only in 19-month-old Tg mice (0.98 ± 0.02 vs. 0.86 ± 0.02), which was confirmed by post-mortem immunohistochemical staining using CD68 as microglial marker. In addition to hippocampus (1.8-fold higher CD68 density based on immunohistochemical staining), increased microglial density was found in striatum (2.3 fold) and cortex (5.6 fold), and CD68 density correlated with [^{18}F]DPA-714 SUVr in these areas [33].

In contrast, a longitudinal study in APP$^{L/S}$ Tg and wt mice using [^{18}F]PBR06 showed significant differences in whole brain tracer uptake between both groups of mice aged 14 months and older (14-15 months: 1.51 ± 0.08 %ID/g vs 1.28 ± 0.05 %ID/g; 15-16 months: 1.41 ± 0.06 %ID/g vs. 1.06 ± 0.10 %ID/g) [34]. This difference was also seen in smaller ROIs, i.e. cortex and hippocampus. Pre-treatment with 1 mg/kg *(R)*-PK11195 led to a decrease in tracer uptake (52% reduction compared with baseline data), showing specific binding to TSPO. In both 5- to 6- and 9- to 10-month-old mice, no significant difference between Tg and wt mice could be shown using PET [34]. *Ex vivo* autoradiography confirmed the PET results, although already at age 9 to 10 months a difference in [^{18}F]PBR06 binding between Tg and wt mice was observed (cortex/striatum 1.13 ± 0.04 vs. 0.96 ± 0.01; hippocampus/striatum 1.27 ± 0.01 vs. 1.10 ± 0.02). The presence of activated microglia (CD68) and TSPO in 9- to 10- and 15- to 16-month-old Tg mice was confirmed with immunohistochemical staining [34]. The inability to visualize this difference with PET most likely is due to the limited spatial resolution of PET in combination with the small size of the relevant structures, leading to partial volume effects. Interestingly, in autoradiography experiments, significantly higher [^{18}F]PBR06 binding in 15- to 16-month old Tg mice compared with age-matched wt mice was found in choroid plexus [34], which is involved in filtering and producing CSF (its dysfunction is linked to amyloid build-up in AD).

In all TSPO imaging studies mentioned above, significantly increased microglial activation in aged Tg mice could be confirmed with immunohistochemical staining. Although James *et al*. [34] showed an increase in whole brain tracer uptake in Tg mice, other studies failed to observe significant differences between Tg and wt mice with TSPO PET, possibly due to a relatively weak neuroinflammatory response in APP Tg mouse models compared with human disease. As the target for immunohistochemical staining in these studies (CD68) differs from the one for PET (TSPO), this

may lead to some discrepancy in the observation of microglial activation. Furthermore, limited spatial resolution of PET combined with small regions within mouse brain, may lead to partial volume effects, thereby hampering the ability to visualise differences between Tg and wt mice with PET. In addition, as microglia exist in a more activated state upon ageing, thereby displaying altered expression levels of several receptors [35,36], small existing differences between aged Tg rodents and aged wt rodent may be lost.

3.2 Clinical PET research in Alzheimer's disease patients

Imaging of neuroinflammation in AD using TSPO as molecular target has been a research interest for several years. Cagnin *et al*. were the first to show increased (*R*)-[^{11}C]PK11195 binding in AD patients compared with healthy volunteers [37]. In 2008, Edison *et al*. showed cortical microglial activation, but not amyloid load, to be negatively correlated with MMSE score, by subjecting a group of AD patients to both a (*R*)-[^{11}C]PK11195 and a [^{11}C]PIB PET scan [38]. However, since these studies, conflicting results have been obtained in TSPO PET imaging of microglial activation in AD.

To confirm the involvement of microglial activation in AD and mild cognitive impairment (MCI), 19 patients with probable AD, 10 with amnestic MCI (prodromal AD) and 21 healthy volunteers were subjected to (*R*)-[^{11}C]PK11195 PET [31]. ROI-based analysis showed no differences in BP_{ND} between diagnostic groups, and only small clusters of increased (*R*)-[^{11}C]PK11195 binding were found using a voxel-based analysis in bilateral occipital lobes in AD patients compared with healthy volunteers. No differences were found between prodromal AD subjects and healthy volunteers [39]. During follow-up (on average 2.6 years), 7 out of 10 MCI patients had clinically progressed to AD, but at the time of the PET scan, no difference between progressive and stable MCI patients was found. Cognitive test scores showed no significant correlation with BP_{ND} in any brain region [39].

In a cross-sectional study using [^{11}C]PBR28 and partial volume corrected images, increased binding was found in AD patients (n=19) compared with both MCI patients (n=10) and healthy volunteers (n=13) in cortical regions known to be pathologically affected [40]. The highest tracer binding was found in inferior parietal lobule, middle and inferior temporal cortex and precuneus (≥1.5-fold higher in AD vs. healthy volunteers), and no difference between diagnostic groups was found in white matter, cerebellum, striatum and thalamus. As the importance of genotype stratification of patients according to the rs6971 single-nucleotide polymorphism was not known at the start of this study, only 29 out of 42 subjects were genotyped (10 AD patients, 7 MCI patients and 12 healthy volunteers). When only comparing HAB AD and MCI patients with HAB controls, significantly increased tracer binding in inferior parietal cortex in AD patients was observed [40]. In MABs, a

similar trend was found, although differences were not significant. In neither case, MCI patients could be distinguished from healthy volunteers. After partial volume correction and adjustment for genotype, age and education, [^{11}C]PBR28 binding in inferior parietal lobule in MCI and AD patients could be correlated with neuropsychological tests (strongest correlation with Clinical Dementia Rating Scale Sum of Boxes (CDR-SB); r=0.570) [40]. Healthy volunteers were not incorporated in the correlation, even though [^{11}C]PBR28 binding did not significantly differ between MCI patients and healthy volunteers, but CDR-SB did (p = 0.013). Subjects also underwent a [^{11}C]PIB scan to examine the correlation between amyloid load and [^{11}C]PBR28 binding, but despite high [^{11}C]PIB binding and hippocampal atrophy in some MCI patients, no correlation with [^{11}C]PBR28 binding was found [40]. These results seem to suggest that TSPO overexpression may only occur after clinical conversion from MCI to AD. However, as pathological studies [41], as well as previous PET studies [37,38], show microglial activation in MCI patients, it is more likely that [^{11}C]PBR28 is not sensitive enough to detect a signal in MCI [40].In another PET study using [^{11}C]PBR28 in AD patients (n=25), MCI patients (n=11) and healthy volunteers (n=21), all genotyped [42], V_T, calculated using the two-tissue compartment model (2TCM) with arterial input function, was compared with SUVr using cerebellum as pseudo-reference region (region in which TSPO is expressed, but the expression should not differ between groups [40]). Differences in V_T values were not observed between groups, but after correcting for the free fraction in plasma (f_P), AD patients showed higher V_T/f_P values in entorhinal and combined middle and inferior temporal cortices than both MCI patients and controls [42]. Both V_T/f_P and SUV in cerebellum did not differ between patient groups. Using cerebellum as pseudo-reference region, SUVrs for [^{11}C]PBR28 were higher in AD patients than in healthy controls (inferior parietal and combined middle and inferior temporal cortices, precuneus, entorhinal and parahippocampal cortices) and MCI patients (combined middle and inferior temporal cortex) [42]. After genotype correction, statistical significance increased, thereby increasing the number of statistically significant different brain regions. According to the authors, SUVr could substitute for absolute quantification of [^{11}C]PBR28 in discriminating AD patients from MCI patients and healthy controls, avoiding the need for arterial blood sampling [42]. However, although least altered, cerebellum is still affected in clinical progression of AD [43] and therefore substituting V_T with SUVr is likely not suitable for all TSPO tracers. Furthermore, stratification for genotype is still required.

In an earlier study using [^{11}C]DAA1106, tracer binding was shown to be increased in AD patients [44]. The affinity of its fluorine-18 labelled analogue [^{18}F]FEDAA1106 for TSPO is two-fold higher, but Varrone *et al.* did not find evidence of increased uptake in AD patients [45]. Although a trend towards higher V_T and BP_{ND} in AD patients (n=9) was observed compared with healthy volunteers (n=7), these were not significantly different. Slow washout was observed in brain, complicating

quantification of [^{18}F]FEDAA1106 and measurement of radioactivity in blood samples was less accurate due to the required acquisition time of 120-150 min, influencing V_T and BP_{ND} [45]. In addition, high non-specific binding could be an issue [45]. Another fluorine-18 analogue of DAA1106, [^{18}F]FEMPA, displayed a higher signal-to-noise ratio than [^{18}F]FEDAA1106 in non-human primates, and was evaluated by the same group in 10 AD patients (MMSE score ≥20) and 7 healthy volunteers (all genotyped) [46]. Although [^{18}F]FEMPA was rapidly metabolised (<20% intact tracer in plasma 20 min p.i.), significantly higher V_T values (on average 19.5 ± 3.0%) were found in AD HABs compared with healthy control HABs, but not in MABs, confirming the need for stratification of genotype. [^{18}F]FEMPA V_T in cortical, limbic and subcortical regions was only found to be weakly and non-significantly correlated with MMSE score (r = -0.37 – -0.41) [46].

To find a suitable kinetic model for quantification of [^{18}F]DPA-714, AD patients (n=9) and healthy volunteers (n=6) were scanned (two dynamic scans; 0-90 min and 120-150 min after tracer injection) [47]. Six kinetic models were compared, of which the reversible two tissue compartment model with blood volume parameter (2T4k_V_B) best described [^{18}F]DPA-714 kinetics [47]. Comparable values for V_T and K_1 were found for various scan durations, indicating that scan time may be shortened to 60 min. No significant difference was found between plasma input-based distribution volume ratios (DVRs) and simplified reference tissue model (SRTM)-derived BP_{ND} values, suggesting SRTM may be useful for assessment of BP_{ND}, although further validation of the reference region is still required [47]. Comparing V_T and BP_{ND} values in AD patients with those in healthy controls, Golla *et al*. found no significant differences on an individual level, neither regionally nor in whole brain. In addition, no differences on a group level were found, but a limitation of the study was the lack of determination of genotype [47]. In a different analysis of the same data, Golla *et al*. generated BP_{ND} values using receptor parametric mapping (RPM), a basis function implementation of SRTM with grey matter (GM) cerebellum as reference region [48]. These BP_{ND} values were found to correlate well with non-linear regression based estimates. When RPM1 derived BP_{ND} images were used as input for statistical parametric mapping (SPM), differences in [^{18}F]DPA-714 binding between AD patients and healthy volunteers could be identified in small brain regions [48].

Both clinical and preclinical PET studies have shown conflicting results. Although, immunohistochemically, neuroinflammation can be demonstrated, the disability to visualise this using TSPO PET is likely due to low signal-to-noise ratios, caused by low brain uptake and (specific) binding of TSPO tracers in the vasculature as has been suggested before [24]. As a result, correlations of tracer binding with clinical score and protein deposition could not be convincingly

demonstrated. In addition, for second-generation TSPO tracers, stratifying for genotype is necessary for correct interpretation of data.

4. Multiple Sclerosis

Multiple sclerosis (MS) is regarded as both an autoimmune disorder and a neurodegenerative disease. The disease is characterized by demyelination of neuronal axons and can present itself in different forms. In relapse-remitting MS (RRMS), patients can still recover after relapse. At a certain point in the course of the disease, the remitting period is too short for patients to recover and patients develop secondary progressive MS (SPMS). A minority of patients (15%) does not have classical relapses, but immediately enters the progressive phase (primary progressive (PP) MS) [49]. In MS lesions, microglia are thought to contribute to tissue repair and damage, possibly depending on the phenotype, although recently a mixture or continuum of pro- and anti-inflammatory microglia was shown in both pre-active and remyelinating lesions [2]. Apart from PET imaging of demyelination, imaging of neuroinflammation is used to investigate disease progression in MS (recent reviews: [11,18,20]).

4.1 Preclinical PET research in animal models of multiple sclerosis

Several pathological events in MS can be mimicked using different animal models, including demyelinating models and experimental autoimmune encephalomyelitis (EAE). Demyelination is usually induced by injection of endotoxins like lysolecithin (lysophosphatidyl choline (LPC)), cuprizone and ethidium bromide [50], while EAE is generated by e.g. subcutaneous immunization with peptides normally found in the CNS. If the majority of activated microglia is of the pro-inflammatory phenotype, disease course becomes more severe in EAE. Nevertheless, activated microglia have also been found to be involved in remyelination of neuronal axons [2,49].

(*R*)-[^{11}C]PK11195 PET was performed in two different rat models of MS by de Paula Faria *et al*. [51]. In one model, demyelination was induced by injection of 1% LPC in the right striatum and corpus callosum of male Sprague-Dawley rats. At 3 and 7 days after LPC injection, focal uptake of (*R*)-[^{11}C]PK11195 was shown at the injection site (SUV 0.79 and 0.66 at 3 and 7 days p.i., respectively), which was not observed in saline treated animals (SUV 0.43 and 0.48 at 3 and 7 days p.i., respectively) [51]. Lesions could not be shown using [^{18}F]FDG PET. After 4 weeks, (*R*)-[^{11}C]PK11195 uptake in the lesions was close to baseline levels. PET results were shown to correlate well with Iba1 (microglial marker) immunohistochemical staining (r^2=0.73) [51]. In a second model, disease progression and treatment effects were monitored in female dark Agouti rats immunized intradermally at the dorsal tail base with endotoxin-free rat recombinant myelin oligodendrocyte

glycoprotein$_{1\text{-}125}$, inducing EAE [52]. Rats received treatment with either 1 mg/kg dexamethasone (anti-inflammatory drug) or saline intraperitoneally (i.p.). Half of the dexamethasone-treated animals did not show any clinical symptoms, the other half presented only with mild symptoms that had resolved at the time of imaging. Increased (*R*)-[^{11}C]PK11195 uptake was observed in saline-treated animals, compared with dexamethasone-treated animals that had not shown any clinical symptoms [52]. Interestingly, (*R*)-[^{11}C]PK11195 PET did show microglial activation in rats that had shown only mild clinical symptoms, even when these symptoms had disappeared due to dexamethasone treatment [52]. Again, authors confirmed the presence of activated microglia by Iba1 immunohistochemical staining.

In order to quantify microglial activation during relapse-remitting EAE, [^{18}F]PBR111 PET was used in female SJL/J mice immunized with PLP$_{139\text{-}151}$ peptide in both flanks [53]. Mattner *et al*. observed highest [^{18}F]PBR111 uptake (300-1100% increase in EAE mice vs. control mice) in the first relapse episode, before the appearance of clinical symptoms. Brain regions responding first to autoimmune inflammation were olfactory bulbs, hippocampus and cerebellum [53]. Tracer uptake in the second episode was not significantly higher, but in the third episode, a significant increase was again observed. Uptake in all CNS regions decreased to control values in animals that recovered (regained weight, clinical score = 0) and did not enter a second episode, >10d after the first episode [53]. Specificity of [^{18}F]PBR111 binding was confirmed by injection of 1 mg/kg (*R*)-PK11195 prior to radiotracer injection, thereby decreasing tracer uptake in CNS by 50-80%. PET results correlated well with mRNA expression of TSPO, as well as with immunohistochemical staining for TSPO [53].

In a chronic focal EAE rat model mimicking progressive MS, the focal lesion could be well visualised using [^{18}F]GE180 PET, even at 127 days after lesion induction [54]. Animals treated with fingolimod (immunomodulating drug, 0.3 mg/kg daily oral administration) clearly showed reduced [^{18}F]GE180 signal, already at 28 days after the start of treatment. PET results were confirmed by *ex vivo* autoradiography and immunohistochemical staining (Iba1) [54]. Results suggested that PET may serve as a tool in human progressive MS to follow treatment effects on neuroinflammation.

In summary, microglial activation could be shown with TSPO PET in several EAE animal models, possibly due to the more focal character of the lesions and a more severe neuroinflammatory response compared with the APP Tg mouse model. Treatment effects can also be well visualised, which holds promise for monitoring MS treatment in humans.

4.2 Clinical PET research in multiple sclerosis patients

(*R*)-[^{11}C]PK11195 PET was first performed in MS patients by Banati *et al*. [55]. Although an increase in tracer binding was observed in MS patients (8 RRMS, 1 SPMS, 3 PPMS) compared with healthy volunteers, (*R*)-[^{11}C]PK11195 could not be correlated to the severity of the disease [55].

More recently, ten SPMS patients and eight age-matched healthy volunteers were subjected to (*R*)-[^{11}C]PK11195 PET [56]. The DVR of (*R*)-[^{11}C]PK11195 was found to be significantly higher in SPMS compared with healthy controls in the periventricular normal appearing white matter (NAWM; 0.96 vs. 0.86) and thalami (1.19 vs. 1.10). Furthermore, in 57% of the chronic T1 hypointense lesions observed with magnetic resonance imaging (MRI), borders of the lesions showed increased (*R*)-[^{11}C]PK11195 uptake and in active gadolinium-enhanced lesions, increased binding was observed in the core of the lesion [56].

In a study of nine RRMS patients in acute relapse undergoing a [^{18}F]FEDAA1106 PET scan, no significant increase in BP_{ND} or V_T was found compared to healthy volunteers (n=5), not even when RRMS patients were divided into drug-using (n=3) and drug-naive (n=6) [57]. Estimation of BP_{ND} and V_T in lesions detected by gadolinium-enhanced T1 weighted MRI could not be obtained robustly [57], due to limited spatial resolution of the PET camera, as stated by the authors. Failure to observe increased tracer uptake in MS patients may also be due to not taking TSPO polymorphism binding status into account.

In a group of RRMS patients (n=11) and healthy volunteers (n=11), stratified and matched for TSPO rs6971 polymorphism (7 HABs, 2 MABs and 2 LABs in each group), a significant effect of TSPO polymorphism on WM binding of [^{18}F]PBR111 was observed (V_T 3.53 HABs; 3.00 MABs; 1.47 LABs) [58]. A trend towards lower whole WM binding in healthy volunteers was observed. In HAB MS patients, $V^{WM}{}_T$ correlated with disease duration. Increased V_T in WM lesional and perilesional volumes (detected as hyperintense lesions on T2 FLAIR MRI) of MS patients was found, compared with healthy volunteers [58]. Two-third of MRI-defined lesions showed higher [^{18}F]PBR111 uptake relative to NAWM, which is consistent with post-mortem pathology in MS patients. Median test-retest variability of [^{18}F]PBR111 $V^{WM}{}_T$ was 23% across subjects [58]. The study demonstrated the feasibility of visualising MS lesions using TSPO PET, provided TSPO polymorphism is taken into account. Although sample-size was too small for MABs and LABs, results obtained in HABs seem promising and warrant further investigation.

Park *et al*. showed a mean absolute test-retest variability of 7-9% for [^{11}C]PBR28 V_T in stable MS patients (2 HABs, 2 MABs) and healthy volunteers (2 HABs, 2 MABs) [59], but no statistically significant difference was found in V_T values between stable MS patients and healthy volunteers in any ROI, including stable lesions. Although average V_T values for HABs were not significantly higher

than for MABs (24% in whole brain GM; 19% in whole brain WM/NAWM), $SUV_{90\text{-}120\ min}$ was significantly higher in HABs (0.8 ± 0.1 vs. 0.6 ± 0.1 for MABs in whole brain GM; 0.7 ± 0.1 vs. 0.6 ± 0.1 for MABs in whole brain WM/NAWM), mainly due to less intersubject variability [59]. The authors conclude that this finding indicates that a 30 min static scan (starting at 90 min p.i.) may provide individual information on genotype of a subject [59]. However, subject groups are rather small (n=2), therefore this conclusion may be too auspicious. One MS patient with active lesions was scanned, however, focal increase of [^{11}C]PBR28 was observed in areas corresponding to gadolinium-enhanced lesions on MRI only using V_T; $SUV_{90\text{-}120\ min}$ images were too noisy to visualise small active MS lesions [59].

Using several TSPO tracers, neuroinflammation can be visualised more clearly in MS patients compared with AD patientswhich might be due to the presence of focal lesions in MS. Possibly, a more severe neuroinflammatory response occurs in MS compared with AD, as this effect is also observed in EAE animal models compared with APP Tg mice.

5. Stroke

Primary brain damage in stroke includes cell death due to reduced blood flow either caused by rupture of cerebral blood vessels (haemorrhagic stroke) or by thrombotic or embolic occlusion of a cerebral artery (ischaemic stroke). Neuroinflammation is triggered by these primary events and has a crucial role in secondary brain damage [60,61]. Microglial activation occurs in both ischaemic and haemorrhagic stroke, where microglia exhibit their beneficial phagocytic function to clear blood components released into the brain parenchyma. On the other hand, pro-inflammatory microglia may also worsen brain damage by activation of blood-derived leukocytes [60]. In PET imaging of neuroinflammation after stroke, (*R*)-[^{11}C]PK11195 has been used most often (recent reviews: [12,13,21]).

5.1 Preclinical PET research in experimental stroke models

A well-characterized stroke model in either mice or rats is occlusion of the middle cerebral artery (MCAO), leading to both primary and secondary brain damage. In a study with permanent MCAO male Wistar rats, animals were followed-up longitudinally by T2*-weighted MRI and (*R*)-[^{11}C]PK11195 PET [62]. Where MRI showed only small differences in lesion volumes between 7 days and 7 months after ischemia, (*R*)-[^{11}C]PK11195 uptake differed substantially on an individual level, especially at the latest time point [62]. PET showed no microglial activation in the infarct region 7 months post-MCAO, but increased (*R*)-[^{11}C]PK11195 uptake was observed in the ipsilateral thalamus

due to secondary degeneration [62], which is in agreement with previous results obtained in humans [63]. Immunohistochemical staining (CD11b, Iba1, ED1) confirmed high microglia and macrophage density in the ipsilateral thalamus [62]. The same group showed, again in permanent MCAO male Wistar rats, a gradual decrease of (*R*)-[^{11}C]PK11195 uptake at different time points (6, 27 and 55 days) after stroke [64]. A shift of microglial activation was observed from regions adjacent to the infarct lesion (day 6) to the ipsilateral thalamus (day 27) and, finally, to midbrain and pons (day 55). This shift was confirmed with Iba1 immunohistochemical staining [64].

Boutin *et al*. directly compared both [^{18}F]DPA-714 [65] and [^{18}F]GE-180 [66] with (*R*)-[^{11}C]PK11195 in a transient MCAO rat model. Rats were scanned 5-7 days after MCAO with two tracers (either [^{18}F]DPA-714 and *(R)*-[^{11}C]PK11195 or [^{18}F]GE-180 and *(R)*-[^{11}C]PK11195) within 24 hours. Although [^{18}F]DPA-714 uptake in the ischaemic core was not significantly higher than uptake of *(R)*-[^{11}C]PK11195, contralateral uptake was lower for [^{18}F]DPA-714, resulting in a higher core/contralateral ratio (4.66 ± 2.50 for [^{18}F]DPA-714 vs. 3.35 ± 1.21 for *(R)*-[^{11}C]PK11195) [65]. An improved signal-to-noise ratio of [^{18}F]GE-180 (6.1 ± 0.8) compared with (*R*)-[^{11}C]PK11195 (4.0 ± 0.7) was observed, due to higher uptake in the ischaemic core and lower uptake in the contralateral region [66]. [^{18}F]GE-180 binding could be displaced with (*R*)-PK11195, and metabolite analysis showed the tracer to be 94% intact in brain 60 min p.i. (21% intact in plasma) [66]. Immunohistochemical staining using CD11b as microglial marker confirmed presence of activated microglia (or macrophages) in the ischaemic lesion in both studies. Authors state that BBB disruption in this MCAO model, however, could have increased tracer uptake in the damaged region [66]. Therefore, these tracers should also be tested at a later time-point after induction of MCAO, to allow for recovery of the BBB.

In an *ex vivo* autoradiography study in C57BL6/N transient MCAO mice after 96 hours of reperfusion, increased [^{3}H]DPA-714 uptake was detected throughout the whole lesion area [67]. Tracer uptake co-localised with Iba1 staining and no correlation was found between lesion size and BBB impairment [67]. In a study monitoring treatment effects of AMD3100 (a CXCR4 antagonist, suppressing immune cell migration) *in vivo,* Balb/c MCAO mice were followed up until 16 days post stroke by [^{18}F]DPA-714 PET [68]. In untreated control mice, increased [^{18}F]DPA-714 uptake compared with baseline uptake (lesion-to-normal ratio 1.09 ± 0.19) was observed starting from day 3 (1.57 ± 0.17), peaking around day 10 (2.04 ± 0.38) and slowly decreasing until day 16 (1.80 ± 0.30). [^{18}F]DPA-714 uptake co-localised with T2-weighted MRI defined lesions and could be displaced with (*R*)-PK11195. In AMD3100 treated mice, a significant reduction in tracer uptake was observed 3 days post stroke compared with saline-treated mice (lesion-to-normal ratio 1.47 ± 0.14 vs. 1.73 ± 0.36 ($p < 0.05$), respectively), although treatment did not fully block upregulation of TSPO [68]. PET results

were confirmed by Western blot and immunohistochemical staining (TSPO, CD11b, GFAP). Apart from a decrease in neuroinflammation, according to the authors the decrease in [^{18}F]DPA-714 uptake in AMD3100 treated mice may also be due to inhibition of macrophage/leukocyte migration [68]. Minocycline (broad-spectrum antibiotic) treatment was monitored in Balb/c transient MCAO mice using [^{18}F]PBR06 over 22 days [69]. In non-treated MCAO animals (n=9), increased tracer uptake was observed in the lesion compared with the contralateral hemisphere, and no tracer uptake was observed in sham-operated animals. [^{18}F]PBR06 uptake was significantly lower in minocycline-treated animals (47%) compared with non-treated animals (59%), and minocycline restored motor function at 22 days post-stroke [69]. PET results were shown to correlate well with immunohistochemical staining (TSPO ≈ CD68 > CD11b).

A new TSPO tracer, [^{11}C]MBMP (K_i of 0.29 nM), was evaluated in male MCAO rats [70]. PET scans were acquired 7 days post ischaemia. Initial brain uptake (1 min p.i.) was >2% ID/g, but the tracer was rapidly metabolized in plasma leaving 24% intact tracer 30 min p.i. (in brain 83% was still intact 30 min p.i.). However, in both PET and autoradiography experiments, high tracer binding to the MCAO lesion was observed (PET: 1.35 ± 0.12 SUV), that could be almost fully displaced (PET) or blocked (autoradiography) with MBMP and (*R*)-PK11195 [70]. Therefore, in an effort to overcome its fast metabolism, the same group developed two fluorinated analogues of MBMP [71]. Both [^{18}F]FEBMP and [^{18}F]FPBMP showed high initial brain uptake (2.5-3.0% ID/g) using PET and in autoradiography studies a high ipsi- to contralateral ratio was observed (3.1 for [^{18}F]FEBMP and 2.1 for [^{18}F]FPBMP). Metabolite analysis was only performed for [^{18}F]FEBMP, showing rapid metabolism in plasma, whereas in brain still 85-90% of tracer was intact 15-30 min p.i. [71], so improvement of metabolic stability compared with [^{11}C]MBMP was not achieved.

MCAO animals display a focal site of neuroinflammation and TSPO PET imaging seems effective in monitoring both disease progression and treatment effects. In MCAO animals, imaging at later time-points is advised, to allow for recovery of BBB, since at only a few days after MCAO, increased tracer uptake can also be attributed to BBB leakage.

5.2 Clinical PET research in patients with stroke

Even though PET imaging of neuroinflammation started off with research in ischaemic stroke[72], and both primary and secondary brain damage could already be visualised with (*R*)-[^{11}C]PK11195 PET [73,74], in years this review is covering, only one clinical study in stroke patients was reported. In this study, nine patients with a unilateral cerebral infarct involving the medial cerebral artery were subjected to [^{18}F]DPA-714 PET 8 to 18 days after stroke [75]. [^{18}F]DPA-714 uptake did not correlate

with infarct volume as determined by MRI, but displayed a greater region surrounding the lesion, suggesting the extent of the inflammatory response is not related to the volume of the lesion. Although BBB leakage was observed with gadolinium-enhanced MRI, tracer uptake extended beyond the region of BBB breakdown observed on MRI [75]. [^{18}F]DPA-714 uptake in the infarcted region was higher due to slower washout than in the contralateral region. Moreover, the contralateral region was found to be a more suitable reference region than cerebellum [75]. The ipsi- to contralateral uptake ratio found for [^{18}F]DPA-714 (1.14-2.10) was higher than that reported for (*R*)-[^{11}C]PK11195 (1.19-1.51) [75,76], although one has to keep in mind that these are two separate studies and therefore not directly comparable. The higher uptake ratio of [^{18}F]DPA-714 compared with that of (*R*)-[^{11}C]PK11195 is probably mostly due to less non-specific binding, as previously shown in an MCAO animal model [65].

6. Tracer development and evaluation

(*R*)-[^{11}C]PK11195 still is the most used tracer for imaging of TSPO, however it suffers from low brain uptake and high non-specific binding, and thus efforts are being made to find a more suitable PET tracer for TSPO. As TSPO is not only overexpressed in activated microglia, but also in reactive astrocytes [6], TSPO imaging of neuroinflammation may not be suitable for all neurodegenerative diseases. For instance, recently astrocytes were found to be more abundant in AD, whereas microglia were more abundant in MCI [77], and thus it may be difficult (if not impossible) to distinguish MCI from AD using TSPO PET. In addition, visualisation of different microglial phenotypes may elucidate their role in disease onset and progression in neurodegenerative diseases. Therefore, PET ligands binding to other targets of interest for imaging neuroinflammation are being more and more explored.

6.1 Translocator Protein 18 kDa

TSPO is located on the outer membrane of mitochondria, where it is involved in translocation of cholesterol to the inner mitochondrial membrane. Expression of TSPO in normal brain is low (except for the olfactory bulbs), but it significantly increases during reactive gliosis and microglial activation, and as such TSPO is an attractive target for imaging neuroinflammation [4]. Even though already over 80 radiolabelled TSPO ligands have been synthesised (recent reviews: [4,9,14]), efforts are still being made to improve on the original ligand (*R*)-[^{11}C]PK11195, as its brain uptake is rather low and non-specific binding relatively high. However, most second generation TSPO radioligands suffer from binding differences due to TSPO polymorphism. Brouwer *et al*. performed a structure activity relationship (SAR) study [78] focused on finding new TSPO ligands that are insensitive to

polymorphism. The chiral centre, incorporating a methyl group between the ring and the amide (see **19e** and **22a**, fig. 1), is necessary for high TSPO affinity [78]. In addition, for one compound of which enantiomers were separated, the *R*-enantiomer showed 2-fold higher affinity than the *S*-enantiomer. However, all other compounds were tested as racemates. Compounds displaying the highest affinity for rat TSPO were tested in human leukocytes of HABs and LABs. Two compounds were found to be genotype insensitive (**19e** and **22a**) and especially **22a** was reported to present good properties to serve as lead for PET radiotracer development [78], although genotype insensitivity has still to be proven *in vivo*.

Three phenylquinazoline-2-carboxamide analogues of (*R*)-[^{11}C]PK11195, [^{11}C]**7**, [^{11}C]**8** and [^{11}C]**9** (fig. 1), were evaluated *in vivo* using PET in rhesus monkeys [79]. All tracers showed high brain uptake that could be blocked with (*R*)-PK11195, but [^{11}C]**9** showed the lowest specific binding. [^{11}C]**7** was considered to be more favourable for quantification, as the time-activity curve (TAC) remained stable after 120 min, whereas it kept rising for [^{11}C]**8** [79]. *In vivo* metabolism of [^{11}C]**7** was shown to be quite rapid with 50% of intact tracer left at 35 min p.i. in plasma, compared with 50% left at 69 min p.i. for [^{11}C]**8**. Nevertheless, *in vitro* LAB/HAB ratios were lowest for [^{11}C]**7** in human cerebellum and leukocytes [79].

A [^{18}F]DPA-714 PET study in healthy C57BL6J mice showed highest tracer uptake in lungs, heart, kidney, spleen and liver [80]. Uptake could be blocked with DPA-714 and (*R*)-PK11195. No radiometabolites were observed in plasma, brain, lungs, spleen and heart at 60 min p.i. [80]. In an *in vivo* metabolite study in rats and baboons, 15 and 11% , respectively, of [^{18}F]DPA-714 was found to be intact in plasmaat 120 min p.i. [81]. Three main radiometabolites were observed, the major one being [^{18}F]fluoroacetate [81]. [^{18}F]DPA-714 PET was also performed in cynomolgus monkeys that had received a unilateral injection of quinolinic acid (QA) in the left putamen to chemically induce neuroinflammation [82]. Seven days after QA injection, [^{18}F]DPA-714 V_T was increased at the centre of the lesion, and at day 21 the area displaying increased tracer binding was enlarged. Differences in uptake were still visible 49 days after QA injection, although the observed increase was only statistically significant at day 21 (V_T 2.57 ± 0.42 vs 0.97 ± 0.08 contralaterally) [82]. Intact [^{18}F]DPA-714 rapidly decreased in plasma with 20% of intact tracer left at 120 p.i. Immunohistochemical staining showed co-localisation of TSPO and microglial markers (CD68 and CD11b) [82]. A series of DPA-714 ether analogues was synthesised [83] in search of structures with increased affinity for TSPO that, at the same time, are still amenable to radiolabelling with either carbon-11 or fluorine-18. Banister *et al*. then evaluated these ether analogues for their affinity for rat TSPO in a competition binding assay against (*R*)-[^{3}H]PK11195. Phenethyl derivative **28** was shown to have the

highest affinity with a K_i of 0.13 nM [83]. In another study, four fluoroalkynyl analogues of DPA-714 were synthesised, of which DPA-C5yne showed the highest affinity towards TSPO (0.35 nM) [84]. *In vitro* metabolism studies in rat liver microsomes showed four main metabolites, similar to DPA-714, but no defluorination was observed. [^{18}F]DPA-C5yne was evaluated in a rat model of excitotoxin induced neuroinflammation (unilateral striatal injection of α-amino-3-hydroxy-5-methyl-4-isoxazolepropionic acid (AMPA)). Autoradiography studies showed increased binding (that could be blocked with (*R*)-PK11195) in the lesioned striatum and *in vivo* PET displayed a high ipsi-to-contralateral ratio (4.62 ± 0.4) [84,85]. In this same rat model of neuroinflammation, 7 days after injection of AMPA, [^{18}F]PBR102 and [^{18}F]PBR111 were evaluated using PET. Binding potentials were significantly higher in the ipsilateral striatum compared with the contralateral side, and no significant difference between tracers was found [86]. Autoradiography with [^{125}I]CLINDE and immunohistochemical staining confirmed the presence of TSPO, astrocytes (GFAP) and microglia (OX42) in the lesioned striatum. Both [^{18}F]PBR102 and [^{18}F]PBR111 were rapidly metabolised, leaving less than 50% of intact tracer in plasma at 14 min p.i. [86]. In another rat model of excitotoxin induced neuroinflammation, in this case achieved by unilateral striatal injection of lipopolysaccharide (LPS), [^{18}F]GE-180 was compared with (*R*)-[^{11}C]PK11195 [87]. Autoradiography and PET experiments were performed 16 hours after injection of LPS (10 μg) and at this time-point, immunohistochemical staining showed an increase in OX-42 (microglia) and GFAP (astrocytes) positive cells. In autoradiography experiments, both tracers showed significantly increased binding in the LPS injected striatum ($BP_{ex\ vivo}$ 0.76 ± 0.31 for (*R*)-[^{11}C]PK11195 and 1.32 ± 0.13 for [^{18}F]GE-180) compared with saline-injected animals ($BP_{ex\ vivo}$ 0.05 ± 0.02 for (*R*)-[^{11}C]PK11195 and 0.05 ± 0.01 for [^{18}F]GE-180) [87]. In *in vivo* PET experiments, binding potentials were also significantly increased for both tracers ($BP_{in\ vivo}$ 0.47 ± 0.06 for (*R*)-[^{11}C]PK11195 and 0.92 ± 0.07 for [^{18}F]GE-180) compared with saline injected animals ($BP_{in\ vivo}$ = 0.00 for both tracers). $BP_{in\ vivo}$ for [^{18}F]GE-180 was significantly higher than that for (*R*)-[^{11}C]PK11195 [87]. Together with the lower signal-to-noise ratio that was shown in MCAO rats [66], [^{18}F]GE-180 may be a promising new PET tracer targeting TSPO.

In a retrospective analysis of baboon data acquired previously using [^{11}C]PBR28, SUV was compared with V_T [88], and SUV was found not to be consistently representative of specific [^{11}C]PBR28 binding in baboon brain. In a study using [^{11}C]PBR28 in ageing rats however, SUV was reported to show less intersubject variability than V_T [36]. Additional studies will have to prove which PET-based measure should be used for quantification of [^{11}C]PBR28. A radiofluorinated analogue of PBR28, [^{18}F]Fluoromethyl-PBR28, was directly compared with [^{11}C]PBR28 in LPS-induced (50 μg) unilateral neuroinflammation in rats [89]. In a competition assay with (*R*)-[^{3}H]PK11195, K_i's of both compounds

were found to be similar (8.07 nM for PBR28 vs. 8.28 nM for fluoromethyl-PBR28). Both tracers showed good ipsi-to-contralateral uptake ratios, but due to differences in kinetics the highest ratio was more rapidly reached with [^{18}F]fluoromethyl-PBR28 (3.2 at 85 min for [^{11}C]PBR28 vs. 3.4 at 35 min for [^{18}F]fluoromethyl-PBR28) [89]. After co-injection with (*R*)-PK11195 or fluoromethyl-PBR28, uptake was reduced with 67 and 71%, respectively. However, already at 5 min after tracer injection, the amount of intact [^{18}F]fluoromethyl-PBR28 was only 27%. Two radiometabolites were observed on HPLC, and defluorination was observed near the end of the scanning period [89]. As high sensitivity to the TSPO polymorphism was shown for PBR28 [5], this sensitivity can also be expected for fluoromethyl-PBR28. Combined with the rapid metabolism and slight defluorination, [^{18}F]Fluoromethyl-PBR28 is unlikely to outperform other (novel) TSPO tracers.

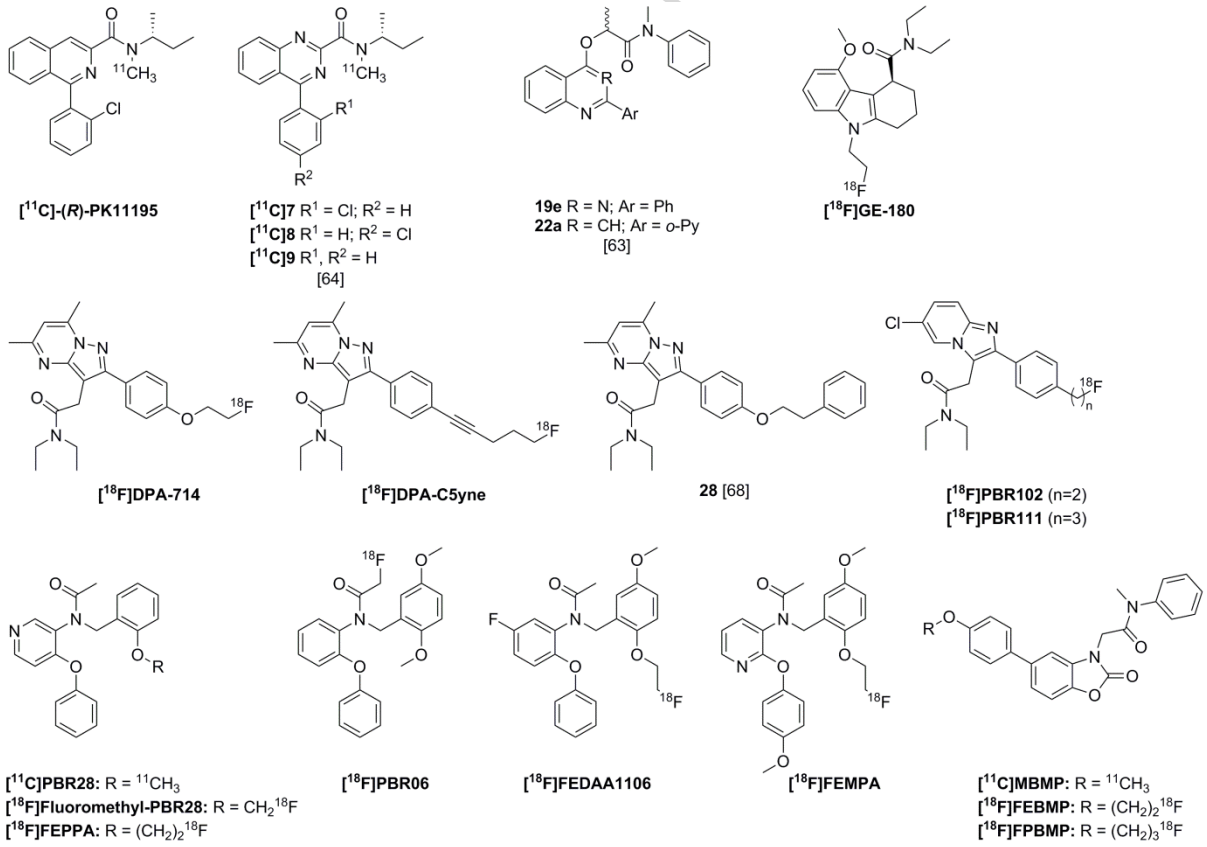

Figure 1: Tracers and ligands targeting TSPO.

6.2 Monoamine oxidase

Monoamine oxidase (MAO) is an outer mitochondrial membrane enzyme that exists in two isoforms: MAO-A and MAO-B. MAO-A is widely expressed in human brain and recently, increased MAO-A activity in brain was demonstrated after systemic LPS administration [90]. Although selective MAO-A tracers are available, even for human use (e.g. [^{11}C]clorgyline, [^{11}C]harmine, [^{11}C]befloxatone (for review: [91]), these were not yet applied in diseases associated with neuroinflammation, but rather

in psychiatric diseases. MAO-B is found predominantly in astrocytes and is thought to contribute to neurodegeneration by disrupting oxidative homeostasis. MAO-B is inhibited by L-deprenyl and MAO-catalysed oxidation displays a strong deuterium isotope effect [16,91]. The rate limiting step in the irreversible binding of L-deprenyl to MAO-B is cleavage of the carbon-hydrogen bond on the alpha position next to the amino group (fig. 2). Cleavage of a carbon-deuterium bond is more difficult due to the higher bond energy; therefore, uptake of deuterated ligands is more dependent on actual MAO-B binding and less dependent on blood flow. Furthermore, deuterated ligands are more slowly metabolised, in general. Taken together, this allows for improved radiotracer quantification [92]. As a consequence, among the first radiotracers reported for MAO-B were [^{11}C]L-deprenyl [93] and its deuterated analogue [^{11}C]deuterium-L-deprenyl ([^{11}C]DED) [92].

Rodriguez-Vieitez *et al*. performed a double tracer study using [^{11}C]DED and [^{11}C]AZD2184 (amyloid tracer) to elucidate the order of events in ageing APPswe Tg mice [94]. APPswe Tg and wt mice were scanned at an age of 8-15 and 18-24 months. APPswe Tg mice were additionally scanned at 6 months of age. [^{11}C]DED SUVr was significantly increased in cortex of 6 month-old Tg mice (0.083 ± 1.094 ± 0.063) compared with 8-15 month-old wt mice (1.036 ± 0.036) [94]. [^{11}C]AZD2184 retention in a combined cortical and hippocampal ROI was significantly higher only in 18- to 24-month-old Tg mice compared with age-matched wt mice, indicating that astrocytosis or neuroinflammation precedes amyloid plaque deposition in APPswe Tg mice [94]. [^{11}C]DED was also used in a study comparing [^{11}C]PIB-positive MCI patients (n=9) with [^{11}C]PIB-negative MCI patients (n=4) and AD patients (n=7) [95]. A significant negative correlation (-0.733) between [^{11}C]DED binding slope and grey matter density (T1 weighted MRI) in the parahippocampus was observed in [^{11}C]PIB-positive MCI patients only, authors suggested that inflammation in the parahippocampus has an effect on grey matter cell loss. No correlation was found between [^{11}C]DED and tau protein levels in the CSF [95]. Both the preclinical and the clinical study using [^{11}C]DED suggest that neuroinflammation, or more precisely astrocytosis, plays a role in the early stages of AD.

Another selective MAO-B tracer, [^{18}F]fluororasagiline, was suspected to have a brain-penetrating metabolite, because radioactivity in the brain was continuously increasing [96]. To enhance the metabolic stability of [^{18}F]fluororasagiline, Nag *et al*. synthesised and evaluated its deuterated analogue ([^{18}F]fluororasagiline-D_2) in cynomolgus monkeys [97]. Rapid brain uptake and faster washout compared with [^{18}F]fluororasagiline was observed with PET, most probably due to deuterium substitution (kinetics comparable to [^{11}C]DED). Binding was decreased with 50% when L-deprenyl (0.5 mg/kg) was administered 30 min prior to tracer injection [97]. Two main metabolites were observed in plasma, and at 15, 45 and 120 min, the amount of intact tracer reduced to 75, 55

and 35%, respectively, compared with 50 and 20% of non-deuterated [^{18}F]fluororasagiline left at 45 and 120 min, respectively [97]. The same group developed two new radiolabelled propargyl amines ([^{18}F]**16** and [^{18}F]**18**, fig. 2) [98]. Autoradiography on healthy human whole hemispheres proved that [^{18}F]**16** binding, but not [^{18}F]**18** binding, could partly be blocked with the MAO-A inhibitor pirlindole, suggesting that [^{18}F]**16** is not selective for MAO-B. Nag *et al*. therefore did not proceed with further evaluation of [^{18}F]**16** [98]. Uptake of [^{18}F]**18** in cynomolgus monkey brain was high and no washout was observed, which may be due to irreversible binding kinetics. Five radiometabolites were observed, leaving only 12% of intact tracer in plasma at 120 p.i. [98]. [^{18}F]**18** distribution in brain differed from e.g. distribution of [^{11}C]DED, which, according to the authors, may be due to brain entrance of radiometabolites [98].

A test-retest and metabolite study was performed by Rusjan *et al.,* using the selective and reversible MAO-B tracer [^{11}C]SL25.1188 in 7 healthy volunteers (19-49 years old) [99]. High brain uptake was observed, and the order of uptake (V_T, 2TCM) was reported as caudate>thalamus>putamen>anterior cingulate>cortex≈temporal cortex≈pons>cerebellar cortex. A retest scan was performed 5 weeks after the first scan and order of uptake remained the same, showing good reproducibility [99]. One radiometabolite was observed, and more than 70% of [^{11}C]SL25.1188 was still intact in plasma 80 min p.i. [99]. Because equilibration of cerebral uptake of [^{11}C]SL25.1188 was slow, a fluorine-18 labelled analogue was developed to allow for longer scan durations [100]. High initial brain uptake and rapid washout was observed in rats. Uptake in bone increased, suggesting substantial defluorination. In rat plasma, only 33% of intact tracer was left 40 min p.i., while 65% of radioactivity in plasma was most likely free fluoride [100]. Furthermore, tracer uptake could not be blocked with L-deprenyl, and *in vitro*, selectivity over MAO-A was not as high as for the original compound. Therefore, authors state that this tracer will not be further evaluated. As the authors have shown that analogues with an elongated fluoroalkyl chain were more selective for MAO-B, radiolabelling of these analogues is currently ongoing [100].

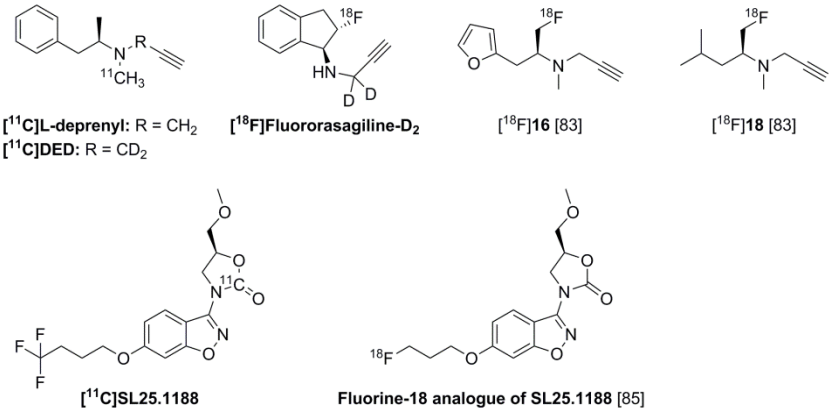

Figure 2: Tracers targeting MAO-B.

6.3 Adenosine receptors

Adenosine receptors are G-protein coupled receptors that bind the endogenous neuromodulator adenosine. Adenosine A_1 receptors (A_1R) are involved in microglial responses and adenosine A_{2A} receptors ($A_{2A}R$) are considered to have a central role in the pathophysiology of neurodegeneration [101].

The A_1R tracer [^{11}C]MPDX (fig. 3) was evaluated in an animal model of neuroinflammation, in which rats were infected with herpes simplex virus 1 (HSV-1) intranasally [102]. Increased [^{11}C]MPDX uptake was observed in hippocampus, cerebellum and medulla of HSV-1-infected, but not in sham-infected animals and this uptake correlated with immunohistochemical staining. Animals with disease score 1 (ruffled fur, dried oral and nasal secretions on the fur, loss of weight) showed the highest uptake, whereas uptake in animals with disease score 2 (hunched posture, increased aggression, paralysis symptoms in the posterior part of the abdomen) seemed to be similar to that in healthy conditions, supporting the hypothesis that A_1R is upregulated in the acute phase of encephalitis [102]. In a previous study by the same group using different TSPO tracers ((*R*)-[^{11}C]PK11195, [^{11}C]DPA-713, [^{18}F]DPA-714 and [^{11}C]DAA1106), neuroinflammation could be shown in all HSV-1 infected animals (no distinction was made between disease scores) [103,104]. Paul *et al*. propose a more neuroprotective role of A_1R, explaining the upregulation of A_1R only in the acute phase of encephalitis [102]. In a study in rats using [^{11}C]MPDX and PET, A_1R receptor occupancy could be derived for the antagonist caffeine (66-99%, dose-dependent), but not for the agonist CPA (even at high doses), due to a different binding domain on the receptor [105].

[^{18}F]CPFPX was evaluated in healthy rats by Elmenhorst *et al*., and SRTM was found to be the model of choice for quantification of [^{18}F]CPFPX [106]. Displacement with DPCPX led to 46-96% decrease in [^{18}F]CPFPX, depending on brain region. Authors suggest that the olfactory bulb can be used as reference region, if the high specific binding in this region (45%) is taken into account. Based on B_{max} values obtained from autoradiography and saturation binding studies on rat brain (30-530 fmol/mg tissue) and using SRTM-based BP_{ND}, an *in vivo* K_D of 3.4-3.8 nM could be determined [106]. Subsequently, Kroll *et al*. determined the test-retest variability (n=4) of [^{18}F]CPFPX BP_{ND} [107]. Good reproducibility in rats was observed using SRTM, but test-retest variability (mean 12%) was higher than previously determined in humans [107,108]. Authors attribute the higher test-retest variability in rats to individual differences in (isoflurane) anaesthesia effects and stress in rats. Results between both studies can however not be directly compared, as test-retest variability in BP_{ND} in humans (4.4-9.2%), was determined using 2TCM with cerebellum as reference region [108]. As specific binding in the reference region is relatively high, this may therefore influence test-retest variability in rats using SRTM due to varying levels of tracer binding in the reference region.

The $A_{2A}R$ tracer [^{11}C]TMSX showed good reproducibility of V_T and BP_{ND} in test-retest scans in 5 healthy volunteers (21-27 years old) [109]. For determination of BP_{ND}, centrum semiovale and cerebral cortex could be used as reference region [109], although blocking studies or occupancy studies are still required for validation. [^{11}C]TMSX was evaluated in 8 SPMS patients and 7 healthy volunteers by Rissanen *et al*. [110]. [^{11}C]TMSX was reported to be metabolically stable, with >90% intact tracer in plasma 50 min p.i. [^{11}C]TMSX V_T was significantly increased in NAWM of SPMS patients compared with controls (0.55 ± 0.08 vs 0.45 ± 0.05) and V_T values correlated with expanded disability status scale (EDSS; Pearson's r 0.56), suggesting A_{2A} receptor expression is increased in NAWM of SPMS patients [110]. To circumvent the need for an arterial input function for kinetic modelling, Rissanen *et al*. developed an automated method for the extraction of grey matter reference region using supervised clustering (SCgm), combined with a population-based arterial input function (7 healthy controls, 12 MS patients and 9 patients with Parkinson's disease) [111]. The previously observed increased [^{11}C]TMSX binding in NAWM of SPMS patients could be confirmed using this method, indicating that quantification of [^{11}C]TMSX brain PET images using SCgm could be feasible [111].

Two fluorine containing analogues (**10a** and **10b**; fig. 3) of SCH442416 ($A_{2A}R$ ligand) were identified by Khanapur *et al*. and subsequently radiolabelled [112]. *In vitro* autoradiography showed binding of both tracers to striatum that could be blocked using KW6002 (selective $A_{2A}R$ antagonist). PET studies showed uptake in striatum ($A_{2A}R$ rich region) and Harderian glands [112], which is most probably non-specific binding. Metabolic stability was reported to be similar to that of [^{11}C]SCH442416 (46% parent [^{18}F]**10a** left 60 min p.i. and 66% parent [^{18}F]**10b** left 60 min p.i.). Affinities of both fluorine analogues were slightly lower than that of the lead compound (lead K_i = 0.5 nM, **10a** K_i = 12.4 nM, **10b** K_i = 53.6 nM), but their rapid brain uptake and washout are promising for further evaluation of these tracers in neuroinflammation models [112]. Disadvantages of [^{11}C]TMSX and [^{11}C]SCH442416, however, are low binding potentials and high levels of non-specific binding. Although preladenant showed no clinical efficacy, this is not an issue for its use as a PET tracer, as preladenant was shown to have high affinity for $A_{2A}R$ (K_i = 1.1 nM), is highly selective and readily crosses the BBB [113]. Therefore, Zhou *et al.* labelled preladenant with carbon-11. Autoradiography showed high binding in striatum that could be blocked with KW6002. During PET experiments in rats, rapid brain uptake was observed and metabolite analysis showed 49% of [^{11}C]preladenant to be intact in plasma 60 min p.i. [113]. Barret *et* al. developed a fluorinated preladenant analogue, [^{18}F]MNI-444, and evaluated it in rhesus monkeys [114]. Metabolite analysis of plasma revealed 45% and 10-15% of tracer to be intact

30 and 120 min p.i., respectively, and no defluorination was reported. Consistent with the A_{2A} receptor distribution in brain, high uptake in striatum was observed. A striatum-to-cerebellum ratio of 12 was reached at 60-70 min p.i., which is stated to be superior to other A_{2A} receptor radioligands reported so far (1.5-2.2) [114]. BP_{ND} (SRTM) was 9.64 ± 1.94 and test-retest variability was below 10%. Furthermore, receptor occupancy of preladenant and tozadenant could be assessed accurately using SRTM or non-invasive Logan graphical analysis without arterial sampling [114].

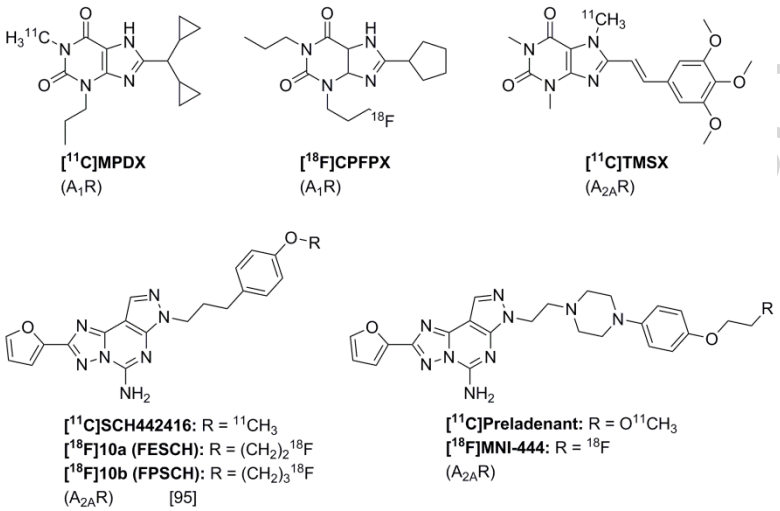

Figure 3: Tracers targeting adenosine receptors.

6.4 Cannabinoid receptor type 2

The cannabinoid receptor type 2 (CB2) is a G-protein coupled receptor that is expressed mainly on immune cells. Under normal conditions expression of CB2 in brain and CNS is low. Although its role in neuroinflammation is not fully understood yet, CB2 receptor expression is expected to increase 10- to 100-fold under neuroinflammatory conditions [115,116].

A series of highly potent and selective CB2 inverse agonists were developed by Gao *et al*. [117]. One of these compounds (**3c**; K_i CB2 = 0.5 nM; K_i CB1 = 1297 nM) was successfully radiolabelled via [^{11}C]methylation, but no further preclinical evaluation has been performed to date [117].

Fluorinated derivatives of a series of CB2 agonists were designed by Lueg *et al*. and the affinity for CB2 was determined in a competition assay with [^{3}H]CP-55940 [118]. Compounds displaying the highest affinity for CB2 were then tested for selectivity over CB1, and **20a** (K_i = 5.8 nM, selectivity over CB1 >200) was subsequently radiolabelled [118,119]. ^{18}F-fluorination was established at two positions ([^{18}F]**1** (**20a**) and [^{18}F]**2**, fig. 4), and only slight defluorination of [^{18}F]**1** was reported in Tris-HCl, EtOH, 0.9% NaCl and Dulbecco's phosphate buffer at 40 ºC for 90 min. Both tracers entered the mouse brain, but pre-treatment with the inverse agonist SR144528 could not reduce uptake significantly in any of the organs investigated (e.g. brain, spleen, lung) [119]. Sixty minutes after tracer injection, only 35% and 43% of [^{18}F]**1** and [^{18}F]**2**, respectively, were found to be intact tracer in

brain [119], indicating a derivative with improved metabolic stability, or at least one with non-brain-penetrating radiometabolites, needs to be developed, even though metabolism may differ between mouse and human.

Mu *et al*. have shown that [^{11}C]KD2 is a selective CB2 agonist (K_i for CB2 = 1.7 nM, K_i for CB1 >10 µM), which was confirmed using autoradiography on rat and mouse spleen (high CB2 expression), as [^{11}C]KD2 binding could be blocked with WIN55212-2 (a full CB agonist), as well as with the selective CB2 agonist GW405833 [120]. Autoradiography on post-mortem spinal cord of amyotrophic lateral sclerosis (ALS) patients also showed high binding of [^{11}C]KD2, which could again be blocked with GW405833. An *in vivo* PET experiment in rats showed high tracer uptake in spleen, liver and intestines. Maximal SUVs (0.2-0.5) in brain were reached at 8-20 min p.i., but blocking experiments with GW405833 (1.5 mg/kg, i.v.) to verify whether brain uptake was CB2 related were inconclusive [120]. Furthermore, high plasma protein binding was observed *in vitro* in human plasma, which is not ideal for a (brain) PET tracer, because of competition of plasma protein binding with BBB passage [120]. Slavik *et al*. performed SAR studies with a series of novel 4-oxo-quinoline derivatives, of which RS-016 (a KD2 analogue, fig. 4) showed the highest binding affinity for CB2 (0.7 nM) and high selectivity over CB1 [116]. Therefore, [^{11}C]RS-016 was developed and shown to be stable *in vitro* in both rodent and human plasma for 40 min. *In vivo* metabolite analysis in rats revealed one more hydrophilic radiometabolite, and 47% of intact tracer was found in plasma at 20 min p.i. [116]. The group performed autoradiography on rodent spleen and human ALS spinal cord and binding of [^{11}C]RS-016 was shown to be specific, as it could be blocked with GW405833. Autoradiography studies and PET imaging of mice injected with LPS (10 mg/kg, i.p.) showed higher [^{11}C]RS-016 binding compared with vehicle injected mice [116]. Further evaluation in different animal models of neuroinflammation is ongoing. Next to 4-oxoquinoline derivatives, in the same group, a 2-oxoquinoline derivative (KP23) with a binding affinity towards CB2 of 6.8 nM (>10 µM for CB1) was selected for radiolabelling [115]. Mu *et al*. performed autoradiography with [^{11}C]KP23 on rodent spleen, showing high binding that could be blocked with GW405833, but also relatively high non-specific binding was observed [115]. PET in healthy rats showed high uptake in spleen, liver and intestines, and low uptake in brain. Three radiometabolites were reported, and intact [^{11}C]KP23 decreased to 25% at 30 min p.i. in plasma [115]. From a series of pyridine analogues developed by the same group, RSR-056 was selected for radiolabelling, based on the high binding affinity (K_i = 4.4 nM) towards human CB2 and high selectivity over CB1 [121]. Autoradiography on rodent spleen showed high binding of [^{11}C]RS-056 that could be blocked with GW405833. In rats, only 21% of tracer was intact in plasma 20 min p.i. Brain uptake in healthy rats was low, but increased uptake was observed in LPS injected mice compared with healthy mice [121].

Hortala *et al.* developed deuterated agonist [^{18}F]**-d$_2$-3** (IC_{50} CB2 =1.4 nM; IC_{50} CB1 = 180 nM), and reported good brain penetration in mice and non-human primates (Rhesus macaque and baboon) [122]. Baboons pre-treated with LPS (0.05-0.1 mg/kg, i.v.) showed an increase of 30% in distribution volume. In Rhesus macaque and baboon, two main radiometabolites were detected and 35% of [^{18}F]**-d$_2$-3** was intact in plasma 180 min p.i. [122]. Specific activity of the tracer was quite low (4.3 GBq/µmol) and selectivity for CB2 over CB1 (~130) was insufficient for PET imaging of CB2 [122].

[^{11}C]NE40 is the first tracer targeting CB2 that was evaluated in human [123]. Whole body biodistribution showed high initial uptake in spleen, which is in line with CB2 expression. Furthermore, Ahmad *et al*. reported fast brain uptake as well as washout in healthy human brain, which might be beneficial for imaging of neuroinflammation [123], although evaluation in patients is warranted.

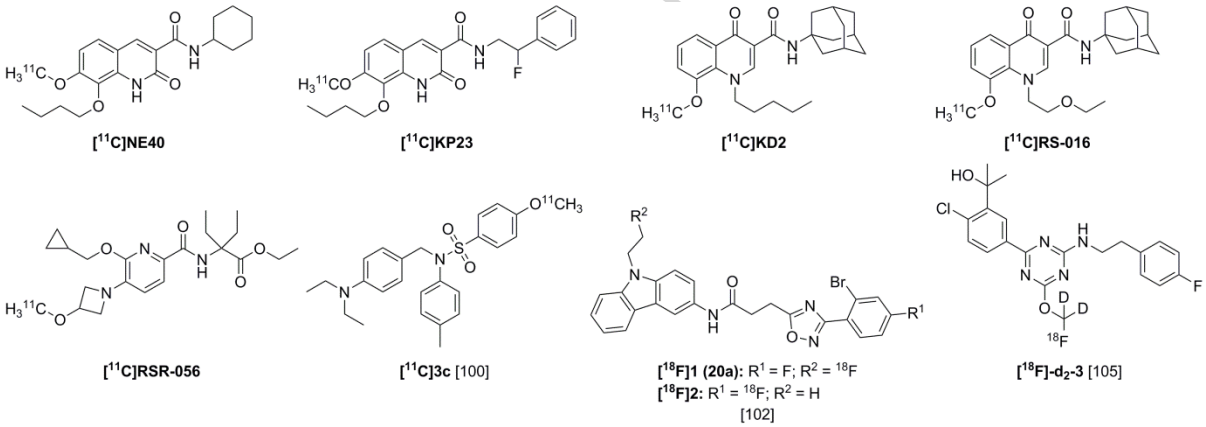

Figure 4: Tracers targeting CB2.

6.5 Cyclooxygenase

Cyclooxygenases are involved in the biosynthesis of prostaglandins via catalysis of the conversion of arachidonic acid into prostaglandin H_2. Prostaglandins regulate, among other things, the neuroinflammatory response. Both COX-1 and COX-2 are inhibited by non-steroidal anti-inflammatory drugs. COX-1 is constitutively expressed, whereas expression of COX-2 is low in normal physiology, but is overexpressed in inflammatory conditions [124].

The selective COX-1 inhibitor ketoprofen displays poor brain entrance due to the presence of a carboxylic acid (fig. 5). To circumvent this, Ohnishi *et al*. developed the radiolabelled methyl ester of ketoprofen ([^{11}C]KTP-Me) and evaluated it in 6 healthy volunteers [125]. Just as in mice, brain uptake was dependent on blood flow, and was followed by rapid washout, probably due to rapid hydrolysis (in plasma complete hydrolysis within 3 min) of [^{11}C]KTP-Me to the carboxylic acid ([^{11}C]ketoprofen) [125]. Brain uptake and retention of [^{11}C]KTP-Me should prove to be sufficient for visualisation of

neuroinflammation in patients, but would be interesting to evaluate, as COX-1 ligands have not been used before to show neuroinflammation in human.

Even though previously COX-2 inhibitor [^{18}F]celecoxib showed extensive defluorination [126], whilst [^{11}C]rofecoxib showed no increased uptake in two models of neuroinflammation [127], Ji *et al*. evaluated [^{11}C]celecoxib and [^{11}C]rofecoxib were *in vitro* and *in vivo* in mice with hypoperfusion induced ischaemia [128]. Hypoperfusion was achieved by unilateral common carotid artery stenosis (placement of a microcoil, 0.18 mm diameter) and complete ligation of the contralateral common carotid artery. Immunohistochemical staining with a COX-2 specific antibody showed presence of COX-2 in the injured neurons, but COX-2 was not found to be expressed on activated glial cells [128]. Autoradiography and PET studies in healthy mouse brain with [^{11}C]celecoxib suggested high non-specific binding, which was confirmed by the disability to block tracer binding with non-radiolabelled celecoxib. Autoradiography with [^{11}C]rofecoxib was only successful at high activity concentrations (11 GBq/L, ~300 nM), which may explain why no increased tracer uptake or retention was observed in *in vivo* PET experiments [128]. According to the authors, it is likely that the affinities of celecoxib (0.04-0.9 µM) and rofecoxib (0.02-0.5 µM) are too low to be successful tracers for PET imaging of COX-2. As there is still a need for selective COX-2 inhibitors with high affinity, Laube *et al*. synthesised and evaluated a series of novel COX-2 inhibitors *in vitro* [124]. Compound **3m** showed selectivity for COX-2 in two different assays, and seems to be a promising candidate for development of a PET tracer [124].

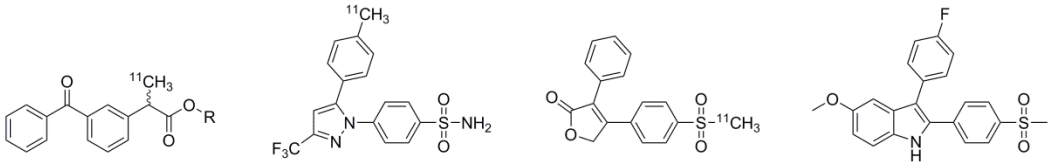

Figure 5: Tracers targeting COX.

6.6 Matrix metalloproteinase 2 and 9

Gelatinases (MMP-2 and MMP-9) have different functions in the CNS, e.g. neurogenesis, regeneration of axons, remyelination and apoptosis. MMPs have also been associated with several neurodegenerative diseases and neuroinflammation [129].

A series of compounds was synthesised by Selivanova *et al*. and tested for affinity against MMP-2, -9 and -1 (collagenase) [130]. Compound **7** (fig. 6), containing a fluorine atom and therefore amenable to radiolabelling, displayed good affinity for MMP-2 and -9 (IC_{50} = 1.8 and 7 nM, respectively) and an IC_{50}>1µM for MMP-1 [130]. *In vitro* studies in rodent and human plasma at 37 ºC showed no

decomposition of [^{18}F]**7** after 2 hours. *In vivo* in mice, only parent was identified 60 min p.i. [130], indicating excellent metabolic stability. Unfortunately, PET studies showed that [^{18}F]**7** did not enter the brain [130]. A less selective MMP inhibitor [^{18}F]**12a** displaying high affinity for MMP-2, -8, -9 and -13 (IC_{50} ranging from 0.05-0.7 nM), showed no radiometabolism upon mouse blood serum incubation for 120 min at 37 ºC [131]. However, *in vivo* in mice, Hugenberg *et al*. reported four radiometabolites in plasma (35% intact tracer 30 min p.i.) and very fast hepatic clearance. Furthermore, PET experiments showed no brain uptake of [^{18}F]**12a** [131]. Thus, some (semi-)selective MMP inhibitors have been radiolabelled, but probably due to structural properties, these compounds do not enter the brain *in vivo* in mice, therefore limiting the use of these tracers for imaging of neuroinflammatory processes.

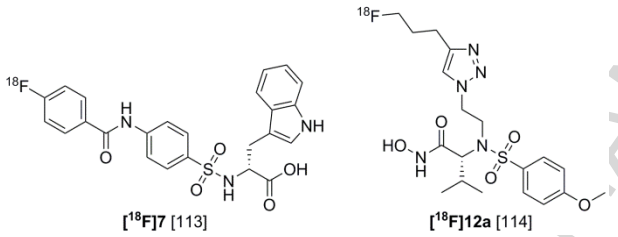

Figure 6: Tracers targeting MMPs.

6.7 Nicotinic acetylcholine receptors

Nicotinic acetylcholine receptors (nAChRs) are ion-gated channels, composed of five subunits, the most abundant subtype in mammalian brain being α4β2. Activation of nAChRs is suggested to be related to suppression of the inflammatory response [132]. In a PET study in MCAO rats by Martín *et al*., 2-[^{18}F]fluoro-A-85380 (fig. 7), a high affinity radioligand for α4β2 nAChRs, was directly compared with (*R*)-[^{11}C]PK11195 [132]. The ipsilateral hemisphere showed increased binding of 2-[^{18}F]fluoro-A-85380 7 days after MCAO and uptake returned to baseline levels at day 28 after MCAO. Using (*R*)-[^{11}C]PK11195, peak uptake also occurred 7 days after MCAO, but declined more slowly until day 28 without returning to baseline values [132]. TSPO and α4β2 nAChRs overexpression in activated microglia was confirmed with immunohistochemical staining. Authors suggest that visualization of α4β2 nAChRs with 2-[^{18}F]fluoro-A-85380 is a promising tool in PET imaging of neuroinflammation [132], however increased (*R*)-[^{11}C]PK11195 uptake could be shown for a longer time after MCAO, indicating a neuroinflammatory response is still present 28 days post-MCAO.

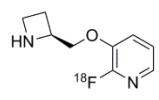

Figure 7: 2-[^{18}F]fluoro-A-85380, targeting α4β2 nAChRs.

6.8 Histamine H_4 receptor

It has been shown that inflammatory stimuli upregulate the histamine H_4 receptor (H_4R) expression on monocytes, and H_4R antagonists have anti-inflammatory effects as the use of H_4R antagonists has suggested a pro-inflammatory role for this receptor in autoimmune diseases [133]. *In vitro*, activation of microglia by histamine and LPS could be demonstrated, and inhibited with H_1R and H_4R antagonists [134,135]. To date, two radioligands have been developed for H_4R, i.e. [^{11}C]JNJ7777120 and [^{11}C]VUF10558 (fig. 8), of which the latter did not show any brain uptake [136,137]. Treatment of EAE mice with JNJ7777120 (8 days, daily administration) exacerbated clinical and neuropathological signs of disease [133]. Although these results do not support the pro-inflammatory role of H_4R, they do suggest a clear effect of H_4R antagonists in disease. Therefore, further evaluation of [^{11}C]JNJ7777120, as well as other novel H_4R radioligands, is warranted and currently ongoing [137].

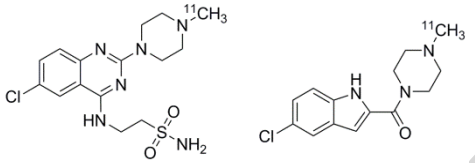

Figure 8: Tracers targeting H_4R.

6.9 $P2X_7$ receptor ($P2X_7R$)

The $P2X_7$ receptor ($P2X_7R$) is thought to play a minimal role in normal physiology and its expression is upregulated on activated microglia [138]. Overexpression of the $P2X_7R$ is associated with the anti-inflammatory microglial phenotype and, therefore, it is an interesting target for PET imaging of neuroinflammation. The $P2X_7R$ antagonist [^{11}C]A-740003 (IC_{50} *h*$P2X_7R$ 40 nM, fig. 9) was synthesised and evaluated in healthy rats [139]. Only low brain uptake was reported, but as $P2X_7R$ expression in normal physiology is low, further evaluation of [^{11}C]A-740003 in animal models of neuroinflammation is still ongoing. A second high affinity $P2X_7R$ radioligand, [^{11}C]GSK1482160 (IC_{50} *h*$P2X_7R$ 3 nM), was synthesised by Gao *et al.,* but has yet to be evaluated *in vivo* [140].

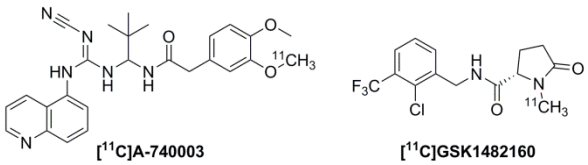

Figure 9: Tracers targeting $P2X_7R$.

7. Summarising comments

In AD, PET imaging of neuroinflammation using TSPO tracers in APP Tg animal models mostly does not show a significant increase in tracer binding compared with wt animals. The same accounts for human AD patients and healthy volunteers, although in some studies, small regional differences in tracer uptake were observed. Since the presence of neuroinflammation has been demonstrated by immunohistochemical staining *ex vivo* many times [41,141], most likely the low signal-to-noise ratios of TSPO PET tracers hamper the visualisation of neuroinflammation *in vivo*. This could be caused by too low expression levels of TSPO due to the relatively mild neuroinflammation, or to pharmacokinetics of the tracers. In addition, microglia and astrocytes are shown to be more abundant in different stages of AD, and as TSPO is overexpressed in both cell types, TSPO tracers might not be suited for clinical diagnosis of MCI or AD.

In MS animal models (EAE), focal lesions could be well visualised using TSPO PET, and treatment effects could also be demonstrated. In MS patients, lesions could be visualised in most studies, applying the same TSPO PET tracers as in AD. This suggests that low signal-to-noise ratios in AD are not caused by the pharmacokinetics of the TSPO PET tracers, but most likely by the low expression levels of TSPO in AD, or the inability to distinguish between microglia and astrocytes.

In stroke animal models, neuroinflammation could be observed up to 55 days after MCAO. One study even showed secondary degeneration (increased uptake in ipsilateral thalamus) 7 months after MCAO. One clinical study using [^{18}F]DPA-714 showed higher tracer uptake in the infarct lesion compared with the contralateral region. The ability to visualise neuroinflammation in stroke using TSPO PET may be attributed to a more severe neuroinflammatory response compared with AD and, therefore, a higher level of TSPO expression.

Up to now, radiotracers targeting TSPO are still mostly used in (clinical) imaging of neuroinflammation. However, TSPO may not be an ideal target due to the polymorphism, resulting in differences in binding affinities of second generation TSPO tracers between genotypes. In addition, expression levels in human disease are low, especially in AD. Significant differences in tracer uptake can be observed in stroke and MS, as long as groups are stratified for genotype. Research to develop new compounds that are insensitive to this polymorphism is ongoing. Radiolabelling of these compounds can afford new TSPO tracers, and may provide an important evolvement in the field.

Next to TSPO, other targets of neuroinflammation are currently under investigation. Using MAO-B tracer [^{11}C]DED, both preclinical and clinical results suggested astrocytosis to precede amyloid deposition in AD. Newly developed MAO-B tracers have not been proven to outperform [^{11}C]DED, but could be useful in the future for early diagnosis of AD.

The hypothesis that A_1R is upregulated in the acute phase of encephalitis in rats was confirmed, and warrants evaluation of this target in other animal models of neuroinflammation. Although with $A_{2A}R$ tracer [^{11}C]TMSX significantly increased uptake in NAWM of MS patients compared with healthy volunteers could be demonstrated, [^{11}C]TMSX suffers from low binding potentials and high non-specific binding. Therefore, other tracers for $A_{2A}R$ have been developed, but are only evaluated in healthy rodents to date. $A_{2A}R$ tracers displaying less non-specific binding could be a valuable tool in imaging of neuroinflammation.

The exact role of CB2 in neuroinflammation should be elucidated, in which PET can play a pivotal role. Recently, the first tracer targeting CB2 was studied in healthy volunteers and use of this tracer in neuroinflammatory pathologies may provide insight in the role of CB2. Several CB2 tracers have only been evaluated in healthy rodents, and too low selectivity for CB2 over CB1 can be an issue for use of these tracers in neuroinflammation imaging.

Tracers developed for COX-2 show either high non-specific binding or too low affinity to be used with PET. Radiolabelled MMP-2 and -9 inhibitors were synthesised and evaluated in healthy animals, but due to structural properties, these tracers did not enter the brain, and are therefore not fitted for imaging of neuroinflammation.

To date, there is no suitable PET radiotracer for either the pro-inflammatory or the anti-inflammatory phenotype of microglia. New targets for imaging that are thought to be specific for one of the microglial phenotypes (α4β2 nAChR, H4R, $P2X_7R$) are emerging, however these still need to be validated. Tracers for these targets are currently investigated preclinical studies and most likely promising ligands will be investigated in human subjects in coming years.

Acknowledgements

Compilation of this review was made possible by funding from the European Union's Seventh Framework Programme (FP7/2007-2013) under grant agreement n° HEALTH-F2-2011-278850 (INMiND).

References

[1] **M.T. Heneka**, M.J. Carson, J. El Khoury, G.E. Landreth, F. Brosseron, D.L. Feinstein, A.H. Jacobs, T. Wyss-Coray, J. Vitorica, R.M. Ransohoff, K. Herrup S.A. Frautschy, B. Finsen, G.C. Brown, A. Verkhratsky, K. Yamanaka, J. Koistinaho, E. Latz, A. Halle, G.C. Petzold, T. Town, D. Morgan, M.L. Shinohara, V.H. Perry, C. Holmes, N.G. Bazan, D.J. Brooks, S. Hunot, B. Joseph, N. Deigendesch, O. Garaschuk, E. Boddeke, C.A. Dinarello, J.C. Breitner, G.M. Cole, D.T. Golenbock, M.P. Kummer, Neuroinflammation in Alzheimer's disease, Lancet Neurol. 14 (2015) 388-405.

[2] **L.A.N. Peferoen**, D.Y.S. Vogel, K. Ummenthum, M. Breur, P.D.A.M. Heijnen, W.H. Gerritsen, R.M.B. Peferoen-Baert, P. van der Valk, C.D. Dijkstra, S. Amor, Activation Status of Human Microglia Is Dependent on Lesion Formation Stage and Remyelination in Multiple Sclerosis, J. Neuropathol. Exp. Neurol. 74 (2015) 48-63.

[3] **S.D. Skaper**, L. Facci, P. Giusti, Mast cells, glia and neuroinflammation: partners in crime? Immunology 141 (2013) 314-327.

[4] **A. Damont**, D. Roeda, F. Dollé, The potential of carbon-11 and fluorine-18 chemistry: illustration through the development of positron emission tomography radioligands targeting the translocator protein 18 kDa, J. Label. Compd. Radiopharm. 56 (2013) 96-104.

[5] **W.C. Kreisl**, K.J. Jenko, C.S. Hines, C. Hyoung Lyoo, W. Corona, C.L. Morse, S.S. Zoghbi, T. Hyde, J.E. Kleinman, V.W. Pike, F.J. McMahon, R.B. Innis, and the Biomarkers Consortium PET Radioligand Project Team. A genetic polymorphism for translocator protein 18 kDa affects both *in vitro* and *in vivo* radioligand binding in human brain to this putative biomarker of neuroinflammation, J. Cereb. Blood Flow Metab. 33 (2013) 53-58.

[6] **R. Rupprecht**, V. Papadopoulos, G. Rammes, T.C. Baghai, J. Fan, N. Akula, G. Groyer, D. Adams, M. Schumacher, Translocator protein (18 kDa) (TSPO) as a therapeutic target for neurological and psychiatric disorders, Nat. Rev. Drug Discovery, 9 (2010) 971-988.

[7] **J.P. Holland**, S.H. Liang, B.H. Rotstein, T.L. Collier, N.A. Stephenson, I. Greguric, N. Vasdev, Alternative approaches for PET radiotracer development in Alzheimer's disease: imaging beyond plaque, J. Label. Compd. Radiopharm. 57 (2014) 323-331.

[8] **C. Hommet**, K. Mondon, V. Camus, M.J. Ribeiro, E. Beaufils, N. Arlicot, P. Corcia, M. Paccalin, F. Minier, T. Gosselin, G. Page, D. Guilloteau, S. Chalon, Neuroinflammation and β Amyloid Deposition in Alzheimer's Disease: In vivo Quantification with Molecular Imaging, Dement. Geriatr. Cogn. Disord. 37 (2014) 1-18.

[9] **S. Venneti**, B.J. Lopresti, C.A. Wiley, Molecular Imaging of Microglia/Macrophages in the Brain, GLIA 61 (2013) 10-23.

[10] **C. Wu**, F. Li, G. Niu, X. Chen, PET Imaging of Inflammation Biomarkers, Theranostics 3 (2013) 448-466.

[11] **D. de Paula Faria**, S. Copray, C. Buchpiguel, R. Dierckx, E. de Vries, PET imaging in multiple sclerosis, J. Neuroimmune Pharmacol. 9 (2014) 468-482.

[12] **W.-D. Heiss**, PET imaging in ischemic cerebrovascular disease: current status and future directions, Neurosci. Bull. 30 (2014) 713-732.

[13] **W.-D. Heiss**, Radionuclide Imaging in Ischemic Stroke, J. Nucl. Med. 55 (2014) 1831-1841.

[14] **G.-J. Liu**, R.J. Middleton, C.R. Hatty, W. Wai-Ying Kam, R. Chan, T. Pham, M. Harrison-Brown, E. Dodson, K. Veale, R.B. Banati, The 18 kDa Translocator Protein, Microglia and Neuroinflammation, Brain Pathol. 24 (2014) 631-653.

[15] **D. Ory**, S. Celen, A. Verbruggen, G. Bormans, PET Radioligands for *In Vivo* Visualization of Neuroinflammation, Curr. Pharm. Des. 20 (2014) 5897-5913.

[16] **E.R. Zimmer**, A. Leuzy, A.L. Benedet, J. Breitner, S. Gauthier, P. Rosa-Neto, Tracking neuroinflammation in Alzheimer's disease: the role of positron emission tomography imaging, J. Neuroinflammation 11 (2014) 120-131.

[17] **H. Barthel**, J. Seibyl, O. Sabri, The role of positron emission tomography imaging in understanding Alzheimer's disease, Expert Rev. Neurother. (2015) doi: 10.1586/14737175.2015.1023296

[18] **F. Niccolini**, P. Su, M. Politis, PET in Multiple Sclerosis, Clin. Nucl. Med. 40 (2015) e46-e52

[19] **J. Varley**, D.J. Brooks, P. Edison, Imaging neuroinflammation in Alzheimer's and other dementias: Recent advances and future directions, Alzheimer's Dementia, (2015) doi: 10.1016/j.jalz.2014.08.105.

[20] **P.M. Matthews**, G. Datta, Positron-emission tomography molecular imaging of glia and myelin in drug discovery for multiple sclerosis, Expert Opin. Drug Discov. 10 (2015) 557-570.

[21] **C. Cerami**, D. Perani, Imaging Neuroinflammation in Ischemic Stroke and in the Atherosclerotic Vascular Disease, Curr. Vasc. Pharmacol. 13 (2015) 218-222.

[22] **D.R. Owen**, Q. Guo, N.J. Kalk, A. Colasanti, D. Kalogiannopoulou, R. Dimber, Y.L. Lewis, V. Libri, J. Barletta, J. Ramada-Magalhaes, A. Kamalakaran, D.J. Nutt, J. Passchier, P.M. Matthews, R.N. Gunn, E.A. Rabiner, Determination of [^{11}C]PBR28 binding potential *in vivo*: a first human TSPO blocking study, J. Cereb. Blood Flow Metab. 34 (2014) 989-994.

[23] **G. Rizzo**, M. Veronese, M. Tonietto, P. Zanotti-Fregonara, F.E. Turkheimer, A. Bertoldo, Kinetic modelling without accounting for the vascular component impairs the quantification of [^{11}C]PBR28 brain PET data, J. Cereb. Blood Flow Metab. 34 (2014) 1060-1069.

[24] **F.E. Turkheimer**, P. Edison, N. Pavese, F. Roncaroli, A.N. Anderson, A. Hammers, A. Gerhard, R. Hinz, Y.F. Tai, D.J. Brooks, Reference and Target Region Modeling of [^{11}C]-(*R*)-PK11195 Brain Studies, J. Nucl. Med. 48 (2007) 158-167.

[25] **Q. Guo**, A. Colasanti, D.R. Owen, M. Onega, A. Kamalakaran, I. Bennacef, P.M. Matthews, E.A. Rabiner, F.E. Turkheimer, R.N. Gunn, Quantification of the Specific Translocator Protein Signal of ^{18}F-PBR111 in Healthy Humans: A Genetic Polymorphism Effect on In Vivo Binding, J. Nucl. Med. 54 (2013) 1915-1923.

[26] **B. Gulyás**, Á. Vas, M. Tóth, A. Takano, A. Varrone, Z. Cselényi, M. Schain, P. Mattsson, C. Halldin, Age and disease related changes in the translocator protein (TSPO) system in the human brain: Positron emission tomography measurements with [^{11}C]vinpocetine, NeuroImage 56 (2011) 1111-1121.

[27] **A. Schuitemaker**, T.F. van der Doef, R. Boellaard, W.M. van der Flier, M. Yaqub, A.D. Windhorst, F. Barkhof, C. Jonker, R.W. Kloet, A.A. Lammertsma, P. Scheltens, B.N.M. van Berckel, Microglial activation in healthy aging, Neurobiol. Aging 33 (2012) 1067-1072.

[28] **A. Kumar**, O. Muzik, V. Shandal, D. Chugani, P. Chakraborty, H.T. Chugani, Evaluation of age-related changes in translocator protein (TSPO) in human brain using ^{11}C-[R]-PK11195 PET, J. Neuroinflammation 9 (2012) 232-241.

[29] **I. Suridjan**, P.M. Rusjan, A.N. Voineskos, T. Selvanathan, E. Setiawan, A.P. Strafella, A.A. Wilson, J.H. Meyer, S. Houle, R. Mizrahi, Neuroinflammation in healthy aging: A PET study using a novel Translocator Protein 18 kDa (TSPO) radioligand, [^{18}F]FEPPA, NeuroImage 84 (2014) 868-875.

[30] **I. Suridjan**, P.M. Rusjan, M. Kenk, N.P.L.G. Verhoeff, A.N. Voineskos, D. Rotenberg, A.A. Wilson, J.H. Meyer, S. Houle, R. Mizrahi, Quantitative Imaging of Neuroinflammation in Human White Matter: A Positron Emission Tomography Study with Translocator Protein 18 kDa Radioligand, [^{18}F]FEPPA, Synapse 68 (2014) 536-547.

[31] **C. Millington**, S. Sonego, N. Karunaweera, A. Rangel, J.R. Aldrich-Wright, I.L. Campbell, E. Gyengesi, G. Münch, Chronic Neuroinflammation in Alzheimer's Disease: New Perspectives on Animal Models and Promising Candidate Drugs, BioMed Res. Int. 2014 (2014) Article ID 309129.

[32] **S. Rapic**, H. Backes, T. Viel, M.P. Kummer, P. Monfared, B. Neumaier, S. Vollmar, M. Hoehn, A. van der Linden, M.T. Heneka, A.H. Jacobs, Imaging microglial activation and glucose consumption in a mouse model of Alzheimer's disease, Neurobiol. Aging 34 (2013) 351-354.

[33] **S. Sérrière,** C. Tauber, J. Vercouillie, C. Mothes, C. Pruckner, D. Guilloteau, M. Kassiou, A. Doméné, L. Garreau, G. Page, S. Chalon, Amyloid load and translocator protein 18 kDa in APPswePS1-dE9 mice: a longitudinal study, Neurobiol. Aging 36 (2015) 1639-1652.

[34] **M.L. James**, N.P. Belichenko, T.-V.V. Nguyen, L.E. Andrews, Z. Ding, H. Liu, D. Bodapati, N. Arksey, B. Shen, Z. Cheng, T. Wyss-Coray, S.S. Gambhir, F.M. Longo, F.T. Chin, Pet Imaging of Translocator Protein (18 kDa) in a Mouse Model of Alzheimer's Disease Using *N*-(2,5,Dimethoxybenzyl)-2-^{18}F-Fluoro-*N*-(2-Phenoxyphenyl)Acetamide, J. Nucl. Med. 56 (2015) 311-316.

[35] **D.M. Norden**, J.P. Godbout, Review: Microglia of the aged brain: primed to be activated and resistant to regulation, Neuropathol. Appl. Neurobiol. 39 (2013) 19-34.

[36] **M.D. Walker**, K. Dinelle, R. Kornelsen, N.V. Lee, Q. Miao, M. Adam, C. Takhar, E. Mak, M. Schulzer, M.J. Farrer, V. Sossi, [^{11}C]PBR28 PET is sensitive to neuroinflammation in the aged rat, J. Cereb. Blood Flow Metab. 35 (2015) 1331-1338.

[37] **A. Cagnin**, D.J. Brooks, A.M. Kennedy, R.N. Gunn, R. Myers, F.E. Turkheimer, T. Jones, R.B. Banati, In-vivo measurement of activated microglia in dementia, Lancet 358 (2001) 461-467.

[38] **P. Edison**, H.A. Archer, A. Gerhard, R. Hinz, N. Pavese, F.E. Turkheimer, A. Hammers, Y.F. Tai, N. Fox, A. Kennedy, M. Rossor, D.J. Brooks, Microglia, amyloid and cognition in Alzheimer's disease: An [11C](R)PK11195-PET and [11C]PIB-PET study, Neurobiol. Dis. 32 (2008) 412-419.

[39] **A. Schuitemaker**, M.A. Kropholler, R. Boellaard, W.M. van der Flier, R.W. Kloet, T.F. van der Doef, D.L. Knol, A.D. Windhorst, G. Luurtsema, F. Barkhof, C. Jonker, A.A. Lammertsma, P. Scheltens, B.N.M. van

Berckel, Microglial activation in Alzheimer's disease: an (*R*)-[^{11}C]PK11195 positron emission tomography study, Neurobiol. Aging 34 (2013) 128-136.

[40] **W.C. Kreisl**, C. Hyoung Lyoo, M. McGwier, J. Snow, K.J. Jenko, N. Kimura, W. Corona, C.L. Morse, S.S. Zoghbi, V.W. Pike, F.J. McMahon, R.S. Turner, R.B. Innis and the Biomarkers Consortium PET Radioligand Project Team, *In vivo* radioligand binding to translocator protein correlates with severity of Alzheimer's disease, Brain 136 (2013) 2228-2238.

[41] **P.L. McGeer**, E.G. McGeer, The amyloid cascade-inflammatory hypothesis of Alzheimer disease: implications for therapy, Acta Neuropathol. 126 (2013) 479-497.

[42] **C.H. Lyoo**, M. Ikawa, J.-S. Liow, S.S. Zoghbi, C.L. Morse, V.W. Pike, M. Fujita, R.B. Innis, W.C. Kreisl, Cerebellum Can Serve As a Pseudo-Reference Region in Alzheimer Disease to Detect Neuroinflammation Measured with PET Radioligand Binding to Translocator Protein, J. Nucl. Med. 56 (2015) 701-706.

[43] **A. Serrano-Pozo**, M.P. Frosch, E. Masliah, B.T. Hyman, Neuropathological alterations in Alzheimer Disease, Cold Spring Harb. Perspect. Med. (2011) 1:a006189.

[44] **F. Yasuno**, M. Ota, J. Kosaka, H. Ito, M. Higuchi, T.K. Doronbekov, S. Nozaki, Y. Fujimura, M. Koeda, T. Asada, T. Suhara, Increased binding of peripheral benzodiazepine receptor in Alzheimer's disease measured by positron emission tomography with [^{11}C]DAA1106, Biol. Psychiatry 64 (2008) 835-841.

[45] **A. Varrone**, P. Mattsson, A. Forsberg, A. Takano, S. Nag, B. Gulyás, J. Borg, R. Boellaard, N. Al-Tawil, M. Eriksdotter, T. Zimmermann, M. Schultze-Mosgau, A. Thiele, A. Hoffmann, A.A. Lammertsma, C. Halldin, In vivo imaging of the 18-kDa translocator protein (TSPO) with [^{18}F]FEDAA1106 and PET does not show increased binding in Alzheimer's disease patients, Eur. J. Nucl. Med. Mol. Imaging 40 (2013) 921-931.

[46] **A. Varrone**, V. Oikonen, A. Forsberg, J. Joutsa, A. Takano, O. Solin, M. Haaparanta-Solin, S. Nag, R. Nakao, N. Al-Tawil, L.A. Wells, E.A. Rabiner, R. Valencia, M. Schultze-Mosgau, A. Thiele, S. Vollmer, T. Dyrks, L. Lehmann, T. Heinrich, A. Hoffmann, A. Nordberg, C. Halldin, J.O. Rinne, Positron emission tomography imaging of the 18-kDa translocator protein (TSPO) with [^{18}F]FEMPA in Alzheimer's disease patients and control subjects, Eur. J. Nucl. Med. Mol. Imaging 42 (2015) 438-446.

[47] **S.S.V. Golla**, R. Boellaard, V. Oikonen, A. Hoffmann, B.N.M. van Berckel, A.D. Windhorst, J. Virta, M. Haaparanta-Solin, P. Luoto, N. Savisto, O. Solin, R. Valencia, A. Thiele, J. Eriksson, R.C. Schuit, A.A. Lammertsma, J.O. Rinne, Quantification of [^{18}F]DPA-714 binding in the human brain: initital studies in healthy controls and Alzheimer's disease patients, J. Cereb. Blood Flow Metab. 35 (2015) 766-772.

[48] **S.S.V. Golla**, R. Boellaard, V. Oikonen, A. Hoffman, B.N.M. van Berckel, A.D. Windhorst, J. Virta, M. Haaparanta-Solin, P. Luoto, N. Savisto, O. Solin, R. Valencia, A. Thiele, J. Eriksson, R.C. Schuit, A.A. Lammertsma, J.O. Rinne, Parametric binding images of the TSPO ligand [^{18}F]DPA-714, The 10th International Symposium on Functional NeuroReceptor Mapping of the Living Brain (2014) O-025, 58.

[49] **E. Ellwardt**, F. Zipp, Molecular mechanisms linking neuroinflammation and neurodegeneration in MS, Exp. Neurol. 262 (2014) 8-17.

[50] **N. Nathoo**, V.W. Yong, J.F. Dunn, Understanding disease processes in multiple sclerosis through magnetic resonance imaging studies in animal models, NeuroImage: Clinical 4 (2014) 743-756.

[51] **D. de Paula Faria**, E.F.J. de Vries, J.W.A. Sijbesma, C.A. Buchpiguel, R.A.J.O. Dierckx, S.C.V.M. Copray, PET imaging of glucose metabolism, neuroinflammation and demyelination in the lysolecithin rat model for multiple sclerosis, Mult. Scler. J. 20 (2014) 1443-1452.

[52] **D. de Paula Faria**, M.L.H. Vlaming, S.C.V.M. Copray, F. Tielen, H.J.A. Anthonijsz, J.W.A. Sijbesma, C.A. Buchpigual, R.A.J.O. Dierckx, J.W.A. van der Hoorn, E.F.J. de Vries, PET Imaging of Disease Progression and Treatment Effects in the Experimental Autoimmune Encephalomyelitis Rat Model, J. Nucl. Med. 55 (2014) 1330-1335.

[53] **F. Mattner**, M. Staykova, P. Berghofer, H.J. Wong, S. Fordham, P. Callaghan, T. Jackson, T. Pham, M.-C. Gregoire, D. Zahra, G. Rahardjo, D. Linares, A. Katsifis, Central Nervous System Expression and PET Imaging of the Translocator Protein in Relapsing-Remitting Experimental Autoimmune Encephalomyelitis, J. Nucl. Med. 54 (2013) 291-298.

[54] **L. Airas**, A.M. Dickens, P. Elo, P. Marjamäki, J. Johansson, O. Eskola, P.A. Jones, W. Trigg, O. Solin, M. Haaparanta-Solin, D.C. Anthony, J. Rinne, In Vivo PET Imaging Demonstrates Diminished Microglial Activation After Fingolimod Treatment in an Animal Model of Multiple Sclerosis, J. Nucl. Med. 56 (2015) 305-310.

[55] **R.B. Banati**, J. Newcombe, R.N. Gunn, A. Cagnin, F. Turkheimer, F. Heppner, G. Price, F. Wegner, G. Giovannoni, D.H. Miller, G.D. Perkin, T. Smith, A.K. Hewson, G. Bydder, G.W. Kreutzberg, T. Joner, M.L. Cuzner, R. Myers, The peripheral benzodiazepine binding site in the brain in multiple sclerosis, Brain 123 (2000) 2321-2337.

[56] **E. Rissanen**, J. Tuiski, J. Rokka, T. Paavilainen, R. Parkkola, J.O. Rinne, L. Airas, In Vivo Detection of Diffuse Inflammation in Secondary Progressive Multiple Sclerosis Using PET Imaging and the Radioligand ^{11}C-PK11195, J. Nucl. Med. 55 (2014) 939-944.

[57] **A. Takano**, F. Piehl, J. Hillert, A. Varrone, S. Nag, B. Gulyás, P. Stenkrona, V.L. Villemagne, C.C. Rowe, R. Macdonell, N. Al Tawil, T. Kucinski, T. Zimmerman, M. Schultze-Mosgau, A. Thiele, C. Halldin, *In vivo* TSPO imaging in patients with multiple sclerosis: a brain PET study with [^{18}F]FEDAA1106, EJNMMI Res. 3 (2013) 30.

[58] **A. Colasanti**, Q. Guo, N. Muhlert, P. Giannetti, M. Onega, R.D. Newbould, O. Ciccarelli, S. Rison, C. Thomas, R. Nicholas, P.A. Muraro, O. Malik, D.R. Owen, P. Piccini, R.N. Gunn, E.A. Rabiner, P.M. Matthews, In Vivo Assessment of Brain White Matter Inflammation in Multiple Sclerosis with ^{18}F-PBR111 PET, J. Nucl. Med. 55 (2014) 1112-1118.

[59] **E. Park**, J.-D. Gallezot, A. Delgadillo, S. Liu, B. Planeta, S.-F. Lin, K.C. O'Connor, K. Lim, J.-Y. Lee, A. Chastre, M.-K. Chen, N. Seneca, D. Leppert, Y. Huang, R.E. Carson, D. Pelletier, ^{11}C-PBR28 imaging in multiple sclerosis patients and healthy controls: test-retest reproducibility and focal visualization of active white matter areas, Eur. J. Nucl. Med. Mol. Imaging 42 (2015) 1081-1092.

[60] **E. Mracsko**, R. Veltkamp, Neuroinflammation after intracerebral haemorrhage, Front. Cell. Neurosci. 8 (2014) 388. doi: 10.3389/fncel.2014.00388

[61] **S. Chen**, Q. Yang, G. Chen, J.H. Zhang, An Update on Inflammation in the Acute Phase of Intracerebral Hemorrhage, Transl. Stroke Res. 6 (2015) 4-8.

[62] **M. Walberer**, S.U. Jantzen, H. Backes, M.A. Rueger, M.H. Keuters, B. Neumaier, M. Hoehn, G.R. Fink, R. Graf, M. Schroeter, *In-vivo* detection of inflammation and neurodegeneration in the chronic phase after permanent embolic stroke in rats, Brain Res. 1581 (2014) 80-88.

[63] **S. Pappata**, M. Levasseur, R.N. Gunn, R. Myers, C. Crouzel, A. Syrota, T. Jones, G.W. Kreutzberg, R.B. Banati, Thalamic microglial activation in ischemic stroke detected in vivo by PET and [^{11}C]PK11195, Neurology 55 (2000) 1052-1054.

[64] **H.L. Walter**, M. Walberer, M.A. Rueger, H. Backes, D. Wiedermann, M. Hoehn, B. Neumaier, R. Graf, G.R. Fink, M. Schroeter, *In Vivo* Analysis of Neuroinflammation in the Late Chronic Phase After Experimental Stroke, Neuroscience 292 (2015) 71-80.

[65] **H. Boutin**, C. Prenant, R. Maroy, J. Galea, A.D. Greenhalgh, A. Smigova, C. Cawthorne, P. Julyan, S.M. Wilkinson, S.D. Banister, G. Brown, K. Herholz, M. Kassiou, N.J. Rothwell, [^{18}F]DPA-714: Direct Comparison with [^{11}C]PK11195 in a Model of Cerebral Ischemia in Rats, PloS ONE 8 (2013) e56441. doi:10.1371/journal.pone.0056441.

[66] **H. Boutin**, K. Murray, J. Pradillo, R. Maroy, A. Smigova, A. Gerhard, P.A. Jones, W. Trigg, ^{18}F-GE-180: a novel TSPO radiotracer compared to ^{11}C-R-PK11195 in a preclinical model of stroke, Eur. J. Nucl. Med. Mol. Imaging 42 (2015) 503-511.

[67] **D. Harhausen**, V. Sudmann, U. Khojasteh, J. Müller, M. Zille, K. Graham, A. Thiele, T. Dyrks, U. Dirnagl, A. Wunder, Specific Imaging of Inflammation with the 18kDa Translocator Protein Ligand DPA-714 in Animal Models of Epilepsy and Stroke, PLoS ONE 8 (2013) e69529. doi:10.1371/journal.pone.0069529.

[68] **Y. Wang**, X. Yue, D.O. Kiesewetter, Z. Wang, J. Lu, G. Niu, G. Teng, X. Chen, [^{18}F]DPA-714 PET Imaging of AMD3100 Treatment in a Mouse Model of Stroke, Mol. Pharmaceutics 11 (2014) 3463-3470.

[69] **F.M. Lartey**, G.-O. Ahn, R. Ali, S. Rosenblum, Z. Miao, N. Arksey, B. Shen, M. Vilalta Colomer, M. Rafat, H. Liu, M.A. Alejandre-Alcazar, J.W. Chen, T. Palmer, F.T. Chin, R. Guzman, B.W. Loo Jr., E. Graves, The Relationship Between Serial [^{18}F]PBR06 PET Imaging of Microglial Activation and Motor Function Following Stroke in Mice, Mol. Imaging Biol. 16 (2014) 821-829.

[70] **A.K. Tiwari**, J. Yui, M. Fujinaga, K. Kumata, Y. Shimoda, T. Yamasaki, L. Xie, A. Hatori, J. Maeda, N. Nengaki, M.-R. Zhang, Characterization of a novel acetamidobenzoxazolone-based PET ligand for translocator protein (18 kDa) imaging of neuroinflammation in the brain, J. Neurochem. 129 (2014) 712-720.

[71] **A.K. Tiwari**, M. Fujinaga, J. Yui, T. Yamasaki, L. Xie, K. Kumata, A.K. Mishra, Y. Shimoda, A. Hatori, B. Ji. M. Ogawa, K. Kawamura, F. Wang, M.-R. Zhang, Synthesis and evaluation of new ^{18}F-labelled acetamidobenzoxazolone-based radioligands for imaging of the translocator protein (18 kDa, TSPO) in the brain, Org. Biomol. Chem. 12 (2014) 9621-9630.

[72] **S.C. Ramsay**, C. Weiller, R. Myers, J.E. Cremer, S.K. Luthra, A.A. Lammertsma, R.S.J. Frackowiak, Monitoring by PET of macrophage accumulation in brain after ischaemic stroke, Lancet 339 (1992) 1054-1055.

[73] **A. Gerhard**, J. Schwarz, R. Myers, R. Wise, R.B. Banati, Evolution of microglial activation in patients after ischemic stroke: a [(11)C](R)-PK11195 PET study. Neuroimage 24 (2005) 591-595.

[74] **B.A. Radlinska**, S.A. Ghinani, P. Lyon, D. Jolly, J.P. Soucy, J. Minuk, R. Schirrmacher, A. Thiel, Multimodal microglia imaging of fiber tracts in acute subcortical stroke, Ann. Neurol. 66 (2009) 825-832.

[75] **M.-J. Ribeiro**, J. Vercouillie, S. Debiais, J.-P. Cottier, I. Bonnaud, C. Camus, S. Banister, M. Kassiou, N. Arlicot, D. Guilloteau Could ^{18}F-DPA-714 PET imaging be interesting to use in the early post-stroke period? EJNMMI Res. 4 (2014) 28.

[76] **A. Gerhard**, B. Neumaier, E. Elitok, G. Glatting, V. Ries, R. Tomczak, A.C. Ludolph, S.N. Reske, In vivo imaging of activated microglia using [^{11}C]PK11195 and positron emission tomography in patients after ischemic stroke, Neuroreport 11 (2000) 2957-2960.

[77] **A. Ekonomou**, G. M. Savva, C. Brayne, G. Forster, P. T. Francis, M. Johnson, E. K. Perry, J. Attems, A. Somani, S. L. Minger, C. G. Ballard, Stage-Specific Changes in Neurogenic and Glial Markers in Alzheimer's Disease, Biol. Psychiatry 77 (2015) 711-719.

[78] **C. Brouwer**, K. Jenko, S.S. Zoghbi, R.B. Innis, V.W. Pike, Development of *N*-Methyl-(2-arylquinolin-4-yl)oxypropanamides as Leads to PET Radioligands for Translocator Protein (18 kDa), J. Med. Chem. 57 (2014) 6240-6251.

[79] **P. Zanotti-Fregonara**, Y. Zhang, K.J. Jenko, R.L. Gladding, S.S. Zoghbi, M. Fujita, G. Sbardella, S. Castellano, S. Taliani, C. Martini, R.B. Innis, F. Da Settimo, V.W. Pike, Synthesis and Evaluation of Translocator 18 kDa Protein (TSPO) Positron Emission Tomography (PET) Radioligands with Low Binding Sensitivity to Human Single Nucleotide Polymorphism rs6971, ACS Chem. Neurosci. 5 (2014) 963-971.

[80] **C. Vicidomini**, M. Panico, A. Greco, S. Gargiulo, A.R.D. Coda, A. Zannetti, M. Gramanzini, G.N. Roviello, M. Quarantelli, B. Alfano, B. Tavitian, F. Dollé, M. Salvatore, A. Brunetti, S. Pappatà, In vivo imaging and characterization of [^{18}F]DPA-714, a potential new TSPO ligand, in mouse brain and peripheral tissues using small-animal PET, Nucl. Med. Biol. 42 (2015) 309-316.

[81] **M.-A. Peyronneau**, W. Saba, S. Goutal, A. Damont, F. Dollé, M. Kassiou, M. Bottlaender, H. Valette, Metabolism and Quantification of [^{18}F]DPA-714, a New TSPO Positron Emission Tomography Radioligand, Drug Metab. Dispos. 41 (2013) 122-131.

[82] **S. Lavisse**, K. Inoue, C. Jan, M.-A. Peyronneau, F. Petit, S. Goutal, J. Dauguet, M. Guillermier, F. Dollé, L. Rbah-Vidal, N. Van Camp, R. Aron-Badin, P. Remy, P. Hantraye, [^{18}F]DPA-714 PET imaging of translocator protein TSPO (18 kDa) in the normal and excitotoxically-lesioned nonhuman primate brain, Eur. J. Nucl. Med. Mol. Imaging 42 (2015) 478-494.

[83] **S.D. Banister**, C. Beinat, S.M. Wilkinson, B. Shen, C. Bartoli, S. Selleri, E. Da Pozzo, C. Martini, F.T. Chin, M. Kassiou, Ether analogues of DPA-714 with subnanomolar affinity for the translocator protein (TSPO), Eur. J. Med. Chem. 93 (2015) 392-400.

[84] **V. Médran-Navarette**, A. Damont, M.-A. Peyronneau, B. Kuhnast, N. Bernards, G. Pottier, F. Marguet, F. Puech, R. Boisgard, F. Dollé, Preparation and evaluation of novel pyrazolo[1,5-*a*]pyrimidine acetamides, closely related to DPA-714, as potent ligands for imaging the TSPO 18 kDa with PET, Bioorg. Med. Chem. Lett. 24 (2014) 1550-1556.

[85] **V. Médran-Navarette**, N. Bernards, B. Kuhnast, A. Damont, G. Pottier, M.-A. Peyronneau, M. Kassiou, F. Marguet, F. Puech, R. Boisgard, F. Dollé, [^{18}F]DPA-C5yne, a novel fluorine-18-labelled analogue of DPA-714: radiosynthesis and preliminary evaluation as a radiotracer for imaging neuroinflammation with PET, J. Label. Compd. Radiopharm. 57 (2014) 410-418.

[86] **P.D. Callaghan**, C.A. Wimberley, G.L. Rahardjo, P.J. Berghofer, T.Q. Pham, T. Jackson, D. Zahra, T. Bourdier, N. Wyatt, I. Greguric, N.R. Howell, R. Siegele, Z. Pastuovic, F. Mattner, C. Loc'h, M.C. Gregoire, A. Katsifis, Comparison of in vivo binding properties of the 18-kDa translocator protein (TSPO) ligands [^{18}F]PBR102 and [^{18}F]PBR111 in a model of excitotoxin-induced neuroinflammation, Eur. J. Nucl. Med. Mol. Imaging 42 (2015) 138-151.

[87] **A.M. Dickens**, S. Vainio, P. Marjamäki, J. Johansson, P. Lehtiniemi, J. Rokka, J. Rinne, O. Solin, M. Haaparanta-Solin, P.A. Jones, W. Trigg, D.C. Anthony, L. Airas, Detection of Microglial Activation in an Acute Model of Neuroinflammation Using PET and Radiotracers ^{11}C-(*R*)-PK11195 and ^{18}F-GE-180, J. Nucl. Med. 55 (2014) 466-472.

[88] **K.K. Yoder**, P.R. Territo, G.D. Hutchins, J. Hannestad, E.D. Morris, J.D. Gallezot, M.D. Normandin, K.P. Cosgrove, Comparison of standardized uptake values with volume of distribution for quantitation of [^{11}C]PBR28 brain uptake, Nucl. Med. Biol. 42 (2015) 305-308.

[89] **B.S. Moon**, B.S. Kim, C. Park, J.H. Jung, Y.W. Lee, H.-Y. Lee, D.Y. Chi, B.C. Lee, S.E. Kim, [^{18}F]Fluoromethyl-PBR28 as a Potential Radiotracer for TSPO: Preclinical comparison with [^{11}C]PBR28 in a Rat Model of Neuroinflammation, Bioconjugate Chem. 25 (2014) 442-450.

[90] **Z. Ming**, C.A. Wotton, R.T. Appleton, J.C. Ching, M.E. Loewen, G. Sawicki, L.K. Bekar, Systemic lipopolysaccharide-mediated alteration of cortical neuromodulation involves increases in monoamine oxidase-A and acetylcholinesterase activity, J. Neuroinflammation 12 (2015) 37-47.

[91] **J.S. Fowler**, J. Logan, E. Shumay, N. Alia-Klein, G.-J. Wang, N.D. Volkow, Monoamine oxidase: radiotracer chemistry and human studies, J. Label. Compd. Radiopharm. 58 (2015) 51-64.

[92] **J.S. Fowler**, A.P. Wolf, R.R. MacGregor, S.L. Dewey, J. Logan, D.J. Schlyer, B. Langstrom, Mechanistic Positron Emission Tomography Studies: Demonstration of a Deuterium Isotope Effect in the Monoamine Oxidase-Catalyzed Binding of [^{11}C]L-Deprenyl in Living Baboon Brain, J. Neurochem. 51 (1988) 1524-1534.

[93] **R.R. MacGregor**, C. Halldin, J.S. Fowler, A.P. Wolf, C.D. Arnett, B. Langström, D. Alexoff, Selective, Irreversible In Vivo Binding of [^{11}C]Clorgyline and [^{11}C]-L-Deprenyl in Mice: Potential for Measurement

of Functional Monoamine Oxidase Activity in Brain Using Positron Emission Tomography, Biochem. Pharmacol. 34 (1985) 3207-3210.

[94] **E. Rodriguez-Vieitez**, R. Ni, B. Gulyás, M. Tóth, J. Häggkvist, C. Halldin, L. Voytenko, A. Marutle, A. Nordberg, Astrocytosis precedes amyloid plaque deposition in Alzheimer APPswe transgenic mouse brain: a correlative positron emission tomography and in vitro imaging study, Eur. J. Nucl. Med. Mol. Imaging 42 (2015) 1119-1132.

[95] **I.H. Choo**, S.F. Carter, M.L. Schöll, A. Nordberg, Astrocytosis measured by ^{11}C-deprenyl PET correlates with decrease in gray matter density in the parahippocampus of prodromal Alzheimer's patients, Eur. J. Nucl. Med. Mol. Imaging 41 (2014) 2120-2126.

[96] **S. Nag**, L. Lehmann, G. Kettschau, T. Heinrich, A. Thiele, A. Varrone, B. Gulyas, C. Halldin, Synthesis and evaluation of [^{18}F]fluororasagiline, a novel positron emission tomography (PET) radioligand for monoamine oxidase B (MAO-B), Bioorg. Med. Chem. 20 (2012) 3065-3071.

[97] **S. Nag**, L. Lehmann, G. Kettschau, M. Toth, T. Heinrich, A. Thiele, A. Varrone, C. Halldin, Development of a novel fluorine-18 labeled deuterated fluororasagiline ([^{18}F]fluororasagiline-D_2) radioligand for PET studies of monoamino oxidase B (MAO-B), Bioorg. Med. Chem. 21 (2013) 6634-6641.

[98] **S. Nag**, G. Kettschau, T. Heinrich, A. Varrone, L. Lehmann, B. Gulyas, A. Thiele, É. Keller, C. Halldin, Synthesis and biological evaluation of novel propargyl amines as potential fluorine-18 labeled radioligands for detection of MAO-B activity, Bioorg. Med. Chem. 21 (2013) 186-195.

[99] **P.M. Rusjan**, A. Wilson, L. Miler, I. Fan, R. Mizrahi, S. Houle, N. Vasdev, J.H. Meyer, Kinetic modelling of the monoamine oxidase B radioligand [^{11}C]SL25.1188 in human brain with high-resolution positron emission tomography, J. Cereb. Blood Flow Metab. 34 (2014) 883-889.

[100] **J.W. Hicks**, O. Sadovski, J. Parkes, S. Houle, B.A. Hay, R.L. Carter, A.A. Wilson, N. Vasdev, Radiosynthesis and ex vivo evaluation of [^{18}F]-(*S*)-3-(6-(3-fluoropropoxy)benzo[*d*]isoxazol-3-yl)-5-(methoxymethyl)oxazolidin-2-one for imaging MAO-B with PET, Bioorg. Med. Chem. Lett. 25 (2015) 288-291.

[101] **A.R. Santiago**, F.I. Baptista, P.F. Santos, G. Cristóvão, A.F. Ambrósio, R.A. Cunha, C.A. Gomes, Role of Microglia Adenosine A_{2A} Receptors in Retinal and Brain Neurodegenerative Diseases, Mediators of Inflammation, 2014 (2014) Article ID 465694.

[102] **S. Paul**, S. Khanapur, W. Boersma, J.W. Sijbesma, K. Ishiwata, P.H. Elsinga, P. Meerlo, J. Doorduin, R.A. Dierckx, A. van Waarde, Cerebral adenosine A_1 receptors are upregulated in rodent encephalitis, NeuroImage 92 (2014) 83-89.

[103] **J. Doorduin**, H.C. Klein, R. A. Dierckx, M. James, M. Kassiou, E.F.J. de Vries, [11C]-DPA-713 and [18F]DPA-714 as New PET Tracers for TSPO: A Comparison with [11C]-(R)-PK11195 in a Rat Model of Herpes Encephalitis, Mol. Imaging Biol. 11 (2009) 386-398.

[104] **J. Doorduin**, H.C. Klein, J.R. de Jong, R.A. Dierckx, E.F.J. de Vries, Evaluation of [11C]DAA1106 for imaging and quantification of neuroinflammation in a rat model of herpes encephalitis, Nuc. Med. Biol. 37 (2010) 9-15.

[105] **S. Paul**, S. Khanapur, J.W. Sijbesma, K. Ishiwata, P.H. Elsinga, P. Meerlo, R.A. Dierckx, A. van Waarde, Use of ^{11}C-MPDX and PET to Study Adenosine A_1 Receptor Occupancy by Nonradioactive Agonists and Antagonists, J. Nucl. Med. 55 (2014) 315-320.

[106] **D. Elmenhorst**, T. Kroll, F. Wedekind, A. Weisshaupt, S. Beer, A. Bauer, In Vivo Kinetic and Steady-State Quantification of ^{18}F-CPFPX Binding to Rat Cerebral A_1 Adenosine Receptors: Validation by Displacement and Autoradiographic Experiments, J. Nucl. Med. 54 (2013) 1411-1419.

[107] **T. Kroll**, D. Elmenhorst, A. Weisshaupt, S. Beer, A. Bauer, Reproducibility of Non-Invasive A_1 Adenosine Receptor Quantification in the Rat Brain Using [^{18}F]CPFPX and Positron Emission Tomography, Mol. Imaging Biol. 16 (2014) 699-709.

[108] **D. Elmenhorst**, P.T. Meyer, A. Matusch, O.H. Winz, K. Zilles, A. Bauer, Test-retest stability of cerebrel A_1 adenosine receptor quantification using [^{18}F]CPFPX and PET, Eur. J. Nucl. Med. Mol. Imaging 34 (2007) 1061-1070.

[109] **M. Naganawa**, M. Mishina, M. Sakata, K. Oda, M. Hiura, K. Ishii, K. Ishiwata, Test-retest variability of adenosine A_{2A} binding in the human brain with ^{11}C-TMSX and PET, EJNMMI Res. 4 (2014) 76.

[110] **E. Rissanen**, J.R. Virta, T. Paavilainen, J. Tuisku, S. Helin, P. Luoto, R. Parkkola, J.O. Rinne, L. Airas, Adenosine A2A receptors in secondary progressive multiple sclerosis: a [^{11}C]TMSX brain PET study, J. Cereb. Blood Flow Metab. 33 (2013) 1394-1401.

[111] **E. Rissanen**, J. Tuiski, P. Luoto, E. Arponen, J. Johansson, V. Oikonen, R. Parkkola, L. Airas, J.O. Rinne, Automated reference region extraction and population-based input function for brain [^{11}C]TMSX PET image analyses, J. Cereb. Blood Flow Metab. 35 (2015) 157-165.

[112] **S. Khanapur**, S. Paul, A. Shah, S. Vatakuti, M.J.B. Koole, R. Zijlma, R.A.J.O. Dierckx, G. Luurtsema, P. Garg, A. van Waarde, P.H. Elsinga, Development of [^{18}F]-Labeled Pyrazolo[4,3-*e*]-1,2,4-triazolo[1,5-*c*]pyrimidine (SCH442416) Analogs for the Imaging of Cerebral Adenosine A_{2A} Receptors with Positron Emission Tomography, J. Med. Chem. 57 (2014) 6765-6780.

[113] **X. Zhou**, S. Khanapur, A.P. Huizing, R. Zijlma, M. Schepers, R.A.J.O Dierckx, A. van Waarde, E.F.J. de Vries, P.H. Elsinga, Synthesis and Preclinical Evaluation of 2-(2-Furanyl)-7-[2-[4-[4-(2-[^{11}C]methoxyethoxy)phenyl]-1-piperazinyl]ethyl]7*H*-pyrazolo[4,3-*e*][1,2,4]triazolo[1,5-*c*]pyrimidine-5-amine ([^{11}C]Preladenant) as a PET Tracer for the Imaging of Cerebral Adenosine A_{2A} Receptors, J. Med. Chem. 57 (2014) 9204-9210.

[114] **O. Barret**, J. Hannestad, D. Alagille, C. Vala, A. Tavares, C. Papin, T. Morley, K. Fowles, H. Lee, J. Seibyl, D. Tytgat, M. Laruelle, G. Tamagnan, Adenosine 2A Receptor Occupancy by Tozadenant and Preladenant in Rhesus Monkeys, J. Nucl. Med. 55 (2014) 1712-1718.

[115] **L. Mu**, R. Slavik, A. Müller, K. Popaj, S. Čermak, M. Weber, R. Schibli, S.D. Krämer, S.M. Ametamey, Synthesis and Preliminary Evaluation of a 2-Oxoquinoline Carboxylic Acid Derivative for PET Imaging the Cannabinoid Type 2 Receptor, Pharmaceuticals 7 (2014) 339-352.

[116] **R. Slavik**, A. Müller Herde, D. Bieri, M. Weber, R. Schibli, S.D. Krämer, S.M. Ametamey, L. Mu, Synthesis, radiolabelling and evaluation of novel 4-oxo-quinoline derivatives as PET tracers for imaging cannabinoid type 2 receptor, Eur. J. Med. Chem. 92 (2015) 554-564.

[117] **M. Gao**, J. Xu, M. Wang, Q.-H. Zheng, Facile and high-yield synthesis of *N*-(4-diethylamino)benzyl-4-[^{11}C]methoxy-*N*-(*p*-tolyl)benzenesulfonamide as a new potential PET selective CB2 radioligand, Appl. Radiat. Isot. 90 (2014) 181-186.

[118] **C. Lueg**, D. Schepmann, R. Günther, P. Brust, B. Wünsch, Development of fluorinated CB_2 receptor agonists for PET studies, Bioorg. Med. Chem. 21 (2013) 7481-7498.

[119] **R. Teodoro**, R.-P. Moldovan, C. Lueg, R. Günther, C.K. Donat, F.-A. Ludwig, S. Fischer, W. Deuther-Conrad, B. Wünsch, P. Brust, Radiofluorination and biological evaluation of *N*-aryl-oxadiazolyl-propionamides as potential radioligands for PET imaging of cannabinoid CB_2 receptors, Org. Med. Chem. Lett. 3 (2013) 11-28.

[120] **L. Mu**, D. Bieri, R. Slavik, K. Drandarov, A. Müller, S. Čermak, M. Weber, R. Schibli, S.D. Krämer, S.M. Ametamey, Radiolabeling and *in vitro*/*in vivo* evaluation of N-(1-adamantyl)-8-methoxy-4-oxo-1-phenyl-1,4-dihydroquinoline-3-carboxamide as a PET probe for imaging cannabinoid type 2 receptor, J. Neurochem. 126 (2013) 616-624.

[121] **R. Slavik**, U. Grether, A. Müller Herde, L. Gobbi, J. Fingerle, C. Ullmer, S.D. Krämer, R. Schibli, L. Mu, S.M. Ametamey, Discovery of a High Affinity and Selective Pyridine Analog as a Potential Positron Emission Tomography Imaging Agent for Cannabinoid Type 2 Receptor, J. Med. Chem. 58 (2015) 4266-4277.

[122] **L. Hortala**, J. Arnaud, P. Roux, D. Oustric, L. Boulu, F. Oury-Donat, P. Avenet, T. Rooney, D. Alagille, O. Barret, G. Tamagnan, F. Barth, Synthesis and preliminary evaluation of a new fluorine-18 labelled triazine derivative for PET imaging of cannabinoid CB2 receptor, Bioorg. Med. Chem. Lett. 24 (2014) 283-287.

[123] **R. Ahmad**, M. Koole, N. Evens, K. Serdons, A. Verbruggen, G. Bormans, K. Van Laere, Whole-Body Biodistribution and Radiation Dosimetry of the Cannabinoid Type 2 Receptor Ligand [^{11}C]NE40 in Healthy Subjects, Mol. Imaging Biol. 15 (2013) 384-390.

[124] **M. Laube**, C. Tondera, S.K. Sharma, N. Bechmann, F.-J. Pietzsch, A. Pigorsch, M. Köckerling, F. Wuest, J. Pietzsch, T. Kniess, 2,3-Diaryl-substituted indole based COX-2 inhibitors as leads for imaging tracer development, RSC Adv. 4 (2014) 38726-38742.

[125] **A. Ohnishi**, M. Senda, T. Yamane, M. Sasaki, T. Mikami, T. Nishio, Y. Ikari, H. Nishida, M. Shukuri, T. Takashima, A. Mawatari, H. Doi, Y. Watanabe, H. Onoe, Human whole-body biodistribution and dosimetry of a new PET tracer, [^{11}C]ketoprofen methyl ester, for imagings of neuroinflammation, Nucl. Med. Biol. 41 (2014) 594-599.

[126] **J. Prabhakaran**, M.D. Underwood, R.V. Parsey, V. Arrango, V.J. Majo, N.R. Simpson, R. van Heertum, J.J. Mann, J.S. Kumar, Synthesis and *in vivo* evaluation of [18F-4-[5-(4-methylphenyl)-3-(trifluoromethyl)-1H-pyrazol-1-yl]benzenesulfonamide as a PET imaging probe for COX-2 expression, Bioorg. Med. Chem. 15 (2015) 1802-1807.

[127] **E.F. de Vries**, J. Doorduin, R.A. Dierckx, A. van Waarde, Evaluation of [(11)C]rofecoxib as PET tracer for cyclooxygenase 2 overexpression in rat models of inflammation, Nucl. Med. Biol. 35 (2008) 35-42.

[128] **B. Ji**, K. Kumata, H. Onoe, H. Kaneko, M.-R. Zhang, C. Seki, M. Ono, M. Shukuri, M. Tokunaga, T. Minamihisamatsu, T. Suhara, M. Higuchi, Assessment of radioligands for PET imaging of cyclooxygenase-2 in an ischemic neuronal injury model, Brain Res. 1533 (2013) 152-162.

[129] **G.A. Rosenberg**, Matrix metalloproteinases and their multiple roles in neurodegenerative diseases, Lancet Neurol. 8 (2009) 205-216.

[130] **S.V. Selivanova**, T. Stellfeld, T.K. Heinrich, A. Müller, S.D. Krämer, P.A. Schubiger, R. Schibli, S.M. Ametamey, B. Vos, J. Meding, M. Bauser, J. Hütter, L.M. Dinkelborg, Design, Synthesis, and Initial Evaluation of a High Affinity Positron Emission Tomography Probe for Imaging Matrix Metalloproteinases 2 and 9, J. Med. Chem. 56 (2013) 4912-4920.

[131] **V. Hugenberg**, B. Riemann, S. Hermann, O. Schober, M. Schäfers, K. Szardenings, A. Lebedev, U. Gangadharmath, H. Kolb, J. Walsh, W. Zhang, K. Kopka, S. Wagner, Inverse 1,2,3-Triazole-1-yl-ethyl Substituted Hydroxamates as Highly Potent Matrix Metalloproteinase Inhibitors: (Radio)synthesis, in Vitro and First in Vivo Evaluation, J. Med. Chem. 56 (2013) 6858-6870.

[132] **A. Martín**, B. Szczupak, V. Gómez-Vallejo, M. Domercq, A. Cano, D. Padro, C. Muñoz, M. Higuchi, C. Matute, J. Llop, *In Vivo* PET Imaging of the α4β2 Nicotinic Acetylcholine Receptor As a Marker for Brain Inflammation after Cerebral Ischemia, J. Neurosci. 35 (2015) 5998-6009.

[133] **M.B. Passani**, C. Ballerini, Histamine and neuroinflammation: insights from murine experimental autoimmune encephalomyelitis, Front. Syst. Neurosci. 6 (2012) 33. doi: 10.3389/fnsys.2012.00032

[134] **R. Ferreira**, T. Santos, J. Gonçalves, G. Baltazar, L. Ferreira, F. Agasse, L. Bernardino, Histamine modulates microglia function, J. Neuroinflammation 9 (2012) 90-105.

[135] **H. Dong**, W. Zhang, X. Zeng, G. Hu, H. Zhang, S. He, S. Zhang, Histamine induces upregulated expression of histamine receptors and increase release of inflammatory mediators from microglia, Mol. Neurobiol. 49 (2014) 1487-1500.

[136] **R. Leurs**, R. Smits, M. Mooijer, I. de Esch, B. Windhorst, Synthesis and *in-vivo* evaluation of human histamine H_4 receptor modulators [^{11}C]JNJ7777120 and [^{11}C]VUF10558 for monitoring inflammatory processes using PET, EHRS XXXVIIth Annual Meeting (2008) P26, 87.

[137] **U. Funke**, D.J. Vugts, B. Janssen, A. Spaans, P.S. Kruijer, A.A. Lammertsma, L.R. Perk, A.D. Windhorst, ^{11}C-labeled and ^{18}F-labeled PET ligands for subtype-specific imaging of histamine receptors in the brain, J. Label. Compd. Radiopharm. 56 (2013) 120-129.

[138] **M. Monif**, G. Burnstock, D. A. Williams, Microglia: Proliferation and activation driven by the P2X7 receptor, Int. J. Biochem. Cell Biol. 42 (2010) 1753-1756.

[139] **B. Janssen**, D.J. Vugts, U. Funke, A. Spaans, R.C. Schuit, E. Kooijman, M. Rongen, L.R. Perk, A.A. Lammertsma, A.D. Windhorst, Synthesis and initial preclinical evaluation of the $P2X_7$ receptor antagonist [^{11}C]A-740003 as a novel tracer of neuroinflammation, J. Label. Compd. Radiopharm. 57 (2014) 509-516.

[140] **M. Gao**, M. Wang, M.A. Green, G.D. Hutchins, Q.-H. Zheng, Synthesis of [^{11}C]GSK1482160 as a new PET agent for targeting $P2X_7$ receptor, Bioorg. Med. Chem. Lett. 25 (2015) 1965-1970.

[141] **P.L. McGeer**, E.G. McGeer, History of innate immunity in neurodegenerative disorders, Front. Pharmacol. 2 (2011) Article 77 1-5.

Table 1: Tracers used for PET imaging of neuroinflammation in Alzheimer's disease, multiple sclerosis and stroke (included in this review).

Target	Tracer	Preclinical	Clinical	References
TSPO	(*R*)-[^{11}C]PK11195	APP/PS1 mice		[32]
		Demyelination rat model		[51]
		EAE rats		[52]
		MCAO rats		[62, 64-66, 132]
			MCI, amnestic MCI, AD patients, HC	[39]
			SPMS patients, HC	[56]
	[^{18}F]DPA-714	APPswePS1dE9 mice		[33]
		MCAO rats		[65]
		MCAO mice		[68]
			AD patients, HC	[47, 48]
			Stroke patients	[75]
	[^{18}F]PBR06	APP$^{L/S}$ mice		[34]
		MCAO mice		[69]
	[^{11}C]PBR28		MCI, AD patients, HC	[40]
			MCI, AD patients, HC	[42]
			MS patients, HC	[59]
	[^{18}F]PBR111	EAE mice		[53]
			RRMS patients, HC	[58]
	[^{18}F]FEDAA1106		AD patients, HC	[45]
			RRMS patients, HC	[57]
	[^{18}F]FEMPA		AD patients, HC	[46]
	[^{18}F]GE180	EAE rats		[54]
		MCAO rats		[66]
	[^{11}C]MBMP	MCAO rats		[70]
	[^{18}F]FEBMP	MCAO rats		[71]
	[^{18}F]FPBMP	MCAO rats		[71]
MAO-B	[^{11}C]DED	APPswe mice		[94]
			MCI patients, AD patients	[95]
A_{2A}R	[^{11}C]TMSX		SPMS patients, HC	[110, 111]
nAChrR α2β4	2[^{18}F]-fluoro-A853380	MCAO rats		[132]

HC = healthy control